Accepted Manuscript

Geological Society, London, Special Publications

The role of subduction in the formation of Pangean oceanic large igneous provinces

Philip J. Heron, Erkan Gün, Grace E. Shephard, Juliane Dannberg, Rene Gassmöller, Erin Martin, Aisha Sharif, Russell N. Pysklywec, R. Damian Nance & J. Brendan Murphy

DOI: https://doi.org/10.1144/SP542-2023-12

To access the most recent version of this article, please click the DOI URL in the line above. When citing this article please include the above DOI.

Received 18 January 2023
Revised 18 April 2023
Accepted 20 April 2023

The role of subduction in the formation of Pangean oceanic large igneous provinces

Philip J. Heron[1*], Erkan Gün[1], Grace E. Shephard[2], Juliane Dannberg[3], Rene Gassmöller[3], Erin Martin[4], Aisha Sharif[1], Russell N. Pysklywec[5], R. Damian Nance[6, 7], and J. Brendan Murphy[8]

[1] *University of Toronto Scarborough, Department of Physical and Environmental Sciences, Toronto, Ontario, Canada*

[2] *Centre for Earth Evolution and Dynamics (CEED), Department of Geosciences, University of Oslo, Oslo, Norway*

[3] *University of Florida, Department of Geological Sciences, Florida, United States*

[4] *School of Earth, Atmosphere and Environment Science, Monash University, Clayton, Victoria, 3800, Australia*

[5] *Department of Earth Sciences, University of Toronto, Toronto, Ontario, M5S 3B1, Canada*

[6] *Department of Geological Sciences, Ohio University, Ohio, 45701, USA*

[7] *Department of Earth & Planetary Sciences, Yale University, Connecticut, 06511, USA*

[8] *Department of Earth Sciences, St Francis Xavier University, Antigonish, Nova Scotia, B2G 2W5, Canada*

ORCID ID: PH, https://orcid.org/0000-0002-4813-0504; EG, https://orcid.org/0000-0003-2320-8253; GS, https://orcid.org/0000-0002-3459-4500; JD, 0000-0003-0357-7115; RG https://orcid.org/0000-0001-7098-8198; ELM, https://orcid.org/0000-0002-6426-3729; RP, https://orcid.org/0000-0002-9670-201X; DN, https://orcid.org/0000-0001-9431-0963; BM 0000-0003-2269-1976

*Corresponding author (e-mail: philip.heron@utoronto.ca)

Abstract

Large igneous provinces (LIPs) have been linked to both surface and deep mantle processes. During the formation, tenure, and breakup of the supercontinent Pangea, there is an increase in emplacement events for both continental and oceanic LIPs. There is currently no clear consensus on the origin of LIPs, but a hypothesis relates their formation to crustal emplacement of hot plume material originating in the deep mantle. The interaction of subducted slabs with the lowermost mantle thermal boundary and subsequent return-flow is a key control on such plume generation. This mechanism has been explored for LIPs below the interior of a supercontinent (i.e., continental LIPs). However, a number of LIPs formed exterior to Pangea (e.g., Ontong Java Plateau), with no consensus on their formation mechanism. Here, we consider the dynamics of supercontinent processes as predicted by numerical models of mantle convection, and analyse whether circum-supercontinent subduction could generate both interior (continental) and exterior (oceanic) deep-mantle plumes. Our numerical models show that subduction related to the supercontinent cycle can reproduce the location and timing of the Ontong Java Plateau, Caribbean LIP, and potentially the Shatsky Rise, by linking the origin of these LIPs to the return-flow that generated deep mantle exterior plumes.

Supplementary material: Numerical code input parameters and animations are available at https://github.com/heronphi/Heron_Super22.

Introduction

Pangea is the most recent supercontinent that has assembled and dispersed over the course of Earth's history (Hoffman, 1997; Dalziel 1991; Hoffman, 1991; Moores, 1991; Torsvik, 2003; Li et al., 2004; 2008; Worsley et al., 1984; Murphy & Nance, 1991; Nance & Murphy, 2013; Nance et al., 1986; Murphy et al., 2009; Murphy et al., 2006; Mitchell et al., 2021). In particular, Pangea was formed during the Carboniferous (~320 Ma; Pastor-Galán, 2022) and broke up from the Jurassic-Cretaceous (~175 Ma) onwards. Although there is no agreement on a formal definition for what constitutes a supercontinent (Pastor-Galán et al., 2019; Heron et al., 2021), the process by which continents amalgamate is well established as part of the life cycle of an ocean (e.g., the Wilson Cycle; Burke & Dewey, 1975; Wilson, 1966). The cycle of supercontinent formation and dispersal, in the context of whole-mantle flow, can be viewed as involving the following steps:

1) Closure of oceans by subduction causes large-scale continental collisions (Fig. 1a). Any interior subduction that yields the assembly of the newly amalgamated landmass terminates (Fig. 1b).

2) Termination of interior subduction related to supercontinent formation changes the dynamics both within and below the supercontinent. The initiation and development of circum-supercontinent exterior subduction zones, and the related descent of oceanic lithosphere into the mantle, disrupts the regional mantle dynamics and produces a return flow that can potentially trigger deep mantle plumes (Tan et al., 2002; McNamara & Zhong, 2005; Davies et al., 2015; Davies et al., 2012; Heron et al., 2015; Heron & Lowman, 2010; Heyn et al., 2020; Dannberg & Gassmöller, 2018).

3) Coupled lithosphere and mantle dynamics ultimately break the landmass up after a period of 100-400 Myr (Condie, 2022), leading to continental dispersal. These dynamics may be related to plate driving forces, including a mantle push force from newly formed plumes beneath the supercontinent and/or slab-pull from circum-supercontinent subduction zones, as well as mantle traction and insulating temperature effects (e.g., McKenzie, 1977; Gurnis et al. 2004; Burke & Dewey, 1973; White & McKenzie, 1989; Hill 1991; Courtillot et al., 1999; Brandl et al., 2013; Tan et al., 2002; Coltice et al., 2007; 2009; Lenardic et al., 2005; 2011).

Ancient deep mantle plumes are thought to have been manifested at the Earth's surface by voluminous magmatism erupted over relatively short geological timescales (typically 1-5 million years) to form large igneous provinces (LIPs) (Burke & Torsvik, 2004), and these LIPs can be found in both oceanic and continental lithosphere. A deep mantle source for such plumes can be inferred from different geological and geophysical lines of evidence including regional domal uplift, which suggests the sub-crustal arrival of buoyant plume material (e.g., Sleep, 1990; Davies, 1999; Sengör, 2001; Rainbird & Ernst, 2001; Saunders et al., 2007). Further, a deep mantle source hypothesis is supported by tomographic images beneath modern hotspots (French & Romanowicz, 2015), deep-mantle geochemical signatures including recycled oceanic lithosphere (Sobolev et al., 2007; Williams et al., 2019), and a potential link to low shear-wave velocity seismic features above the core-mantle boundary (Burke et al., 2008). Alternative interpretations of the origin and source of LIPs have been suggested but remain contested (White & McKenzie, 1989; Coffin & Eldholm, 1994; Ernst, 2014; Ernst et al., 2005; Foulger, 2007; Campbell & Kerr, 2007). Although other mechanisms have the ability to produce LIPs, in this study we concentrate on the role of a deep mantle plume in the formation of a LIP and explore the role of plate tectonics in this process.

Several studies have investigated the temporal, spatial, and geodynamic relationships between LIP activity and plate tectonics (e.g., Yale & Carpenter, 1998; Ernst et al., 2005; Ernst & Bleeker, 2010; Sobolev et al., 2011; Heron et al., 2015; Heyn et al., 2020; Marzoli et al., 2018; Beccaluva et al., 2020; Hastie et al., 2014; Buiter et al., 2014; Glišović & Forte, 2017; Condie et al., 2021). Studies suggest that relatively little LIP activity is associated with the amalgamation stage of the supercontinent cycle (e.g., Yale & Carpenter 1998; Ernst et al. 2005; Ernst & Bleeker 2010). However, after a supercontinent has existed for a period of time (100-200 Myrs, Sobolev et al., 2011), the number of LIPs increases on a global scale (e.g., Yale & Carpenter, 1998; Ernst et al., 2005; Ernst & Bleeker, 2010; Sobolev et al., 2011). For example, approximately 26 LIPs have been emplaced globally since the formation of Pangea (Table 1).

A number of papers have discussed the role of subducting slabs of oceanic lithosphere controlling mantle flow and therefore the position and timing of plumes (Tan et al., 2002; McNamara & Zhong, 2005; Davies et al., 2015; Davies et al., 2012; Heron et al., 2015; Heron & Lowman, 2010; Heyn et al., 2020; Dannberg & Gassmöller, 2018). These studies show that sinking slabs of oceanic lithosphere have the power to stir mantle flow and control the thermal evolution of the mantle, which is of particular interest during amalgamation and advanced breakup phases of the supercontinent cycle, when subduction patterns change on a global scale.

Most of the discussion on the supercontinent cycle and the formation of plumes has been directed at the formation of LIPs and/or the break-up of a (super)continent (see Heron, 2019 for a review). The discussion has focused in particular on the formation of the Central Atlantic Magmatic Province (CAMP) (Marzoli et al., 2018), Karoo (Hastie et al., 2014), and Parana-Etendeka (Beccaluva et al., 2020) LIPs, which may have impacted the opening of the Atlantic, and the Deccan Traps LIP which may have played a role in India's separation from Madagascar (Glišović & Forte, 2017). Although mostly located within oceans today, at the time of their eruption all of these LIPs formed within the interior of Pangea and so were first manifested on Earth's surface within Pangea's circum-supercontinent subduction girdle (Figure 2). Indeed, focused long-term subduction may have been capable of forcing a return flow in the mantle beneath Pangea, thereby producing sub-supercontinental plumes as discussed in a number of previous studies (Zhong et al., 2007; Yoshida, 2008; Li and Zhong, 2009; Heron and Lowman, 2010; 2011). In addition, anomalous material near the core-mantle boundary beneath Africa and the Pacific Ocean, characterized by low shear velocities in seismic tomography (see below), has been indicated as a location for plume generation (e.g., Torsvik et al., 2006; Burke et al., 2008; Torsvik et al., 2008; 2010). In particular, the margins of the African Large Low Shear Velocity Provinces (LLSVP) have been linked to LIP formation within the interior of Pangea (e.g., Torsvik et al., 2010).

However, a number of LIPs that formed after supercontinent amalgamation do not lie within this interior framework. Those in the Pacific Ocean (oceanic LIPs or plateaux), for example, formed outside the supercontinent subduction girdle (i.e., in areas that were exterior to the supercontinent) on plates that were subducting beneath it. LIPs such as the Ontong Java Plateau (Fig. 1c), Caribbean LIP (Fig. 1d), and the Shatsky Rise all formed in provinces exterior to Pangea (Figure 1), yet investigations into their formation in the context of circum-supercontinent subduction are limited.

Here, we test the hypothesis that the formation of mantle plumes and resulting LIPs that are interior (i.e., on the overriding plate) and exterior (i.e., on the subducting plate) to a supercontinent could be

generated by the same subduction setting. This dual-mechanism for plume formation can be conceptualized the following way: the subducting slab pushes oceanic material in the direction of its dip beneath a continent (also referred to as Andean-style subduction) to generate an interior mantle plume through a return flow, whilst the same subduction back flow can also trigger one or several plumes on the oceanward side (i.e., exterior scenario) (Figure 3). Both interior and exterior plumes may be linked to the margin of an LLSVP and in this study we prescribe a thermo-chemical layer that is passive to the mantle flow (rather than fixed in place) in order to isolate the impact of subduction on plume formation.

Several mechanisms have been discussed regarding the formation of exterior (oceanic) LIPs, in particular for the Ontong Java Plateau (Tardundo et al., 1991; Zhang et al., 2020; Isse et al., 2022) and Shatsky Rise (Seger et al., 2016). As a contribution to this discussion, we test the theory for exterior plume formation caused by circum-supercontinent subduction by using numerical experiments of 2D and 3D thermo-chemical mantle convection that investigate the effects of subduction processes related to the supercontinent cycle. We analyse the thermal response of the mantle driven by the evolution of surface tectonics to identify the timing and location of exterior plumes, and link this distribution to the formation of oceanic LIPs following Pangea amalgamation.

Methods

In this section we outline the base numerical model setup, followed by the specific supercontinent process for 2D and 3D modeling. A full description of the numerical model setup can be found in the ASPECT input files provided in the supplementary material.

Numerical model setup

In order to study global mantle convection patterns related to subduction, we conduct 2D experiments with prescribed surface velocities to model the formation of a supercontinent. Computations were done using the ASPECT code version 2.4.0 (see Kronbichler et al., 2012; Bangerth et al., 2022a; 2022b; Heister et al., 2017; Gassmöller et al., 2018; He et al., 2017). ASPECT solves the following set of equations for compressible convection in the Earth's mantle, describing the mass, momentum and energy balance (taking into account adiabatic heating, shear heating, and radiogenic heat production), and the transport of chemical composition:

$$-\nabla \cdot (2\eta \dot{\varepsilon}) + \nabla p = \rho \boldsymbol{g}, (1)$$

$$\nabla \cdot (\rho \boldsymbol{u}) = 0, (2)$$

$$\rho C_p \left(\frac{\partial T}{\partial t} + \boldsymbol{u} \cdot \nabla T\right) - \nabla \cdot k \nabla T = \rho H + 2\eta \dot{\varepsilon} : \dot{\varepsilon} + \alpha T (\boldsymbol{u} \cdot \nabla p), (3)$$

$$\frac{\partial C}{\partial t} + \boldsymbol{u} \cdot \nabla C = 0 \ (4)$$

The equations are solved for velocity **u**, pressure p, temperature T and chemical composition C (e.g., harzburgite or recycled ocean crust). η is the viscosity, $\dot{\varepsilon}$ is the deviatoric strain rate ($\frac{1}{2}(\nabla u + \nabla u^T) - \frac{1}{3}(\nabla \cdot u)\delta_{ij}$), **g** is the gravitational acceleration, ρ is the density, Cp is the specific heat capacity (at constant pressure), k is the thermal conductivity, H is the radiogenic heat production, and α is the thermal expansivity.

Our models begin from an initial condition that has an average mantle temperature gradient and composition that is appropriate for the present-day mantle (Figure 4) as determined by previous studies (e.g., Dannberg & Gassmöller, 2018; Zhang & Li, 2018). The initial mantle temperature is laterally homogeneous, following an adiabatic profile with thermal boundary layers at the top and bottom (Dannberg & Gassmöller, 2018). We fix the surface temperature to 273 K and core-mantle boundary temperature to 3700 K (Figure 4). Although 3700 K is a higher temperature than used in some previous studies (e.g., Zhang & Li, 2018), it is well within the range of uncertainty for the exact present-day value (Nomura, et al., 2014). There is greater uncertainty in historic core-mantle boundary temperature values, with previous studies indicating a higher basal temperature in the Hadean (e.g., 4000 K, O'Neill & Zhang, 2018). However, the change in temperature during the geological timeframe we studied is not significant given the uncertainty in its exact value (Nomura et al., 2014). Consequently, we can prescribe a fixed a value of 3700 K for all times during the simulation (e.g., Lay et al., 2008).

Viscosity in the simulations (Figure 4) is depth- and temperature-dependent (as outlined in Heister et al., 2017) and is based on a published viscosity model incorporating constraints from mineral physics, geoid deformation, and seismic tomography (Steinberger & Calderwood, 2006). The temperature-dependence of the viscosity follows the equation from Steinberger and Calderwood (2006):

$$\eta_{lateral} = \exp\left(\frac{-E\,\Delta T}{n\,R\,T\,T_{ref}}\right) \quad (5),$$

where *E* is the activation energy; *T* is temperature; T_{ref} is the reference temperature profile (e.g., the initial adiabat); $\Delta T = T - T_{ref}$; *R* is the gas constant; and *n* is the stress exponent (*n* = 3.5 above 660 km and *n* = 1 below). *E* is also depth-dependent and varies between 300 and 800 kJ mol^{-1} (Steinberger and Calderwood, 2006). Therefore, the temperature-dependence of viscosity is depth-dependent as well, and for a 100 K increase in temperature, it is approximately a factor of 200 at the surface and a factor of 3000 at the core-mantle boundary.

As this viscosity law produces very strong lateral and vertical viscosity variations over the temperature range appropriate for Earth (ΔT = 3427 K) (Figure 4), we limit the viscosity range to four orders of magnitude to reduce the computation time and make model runs feasible (1×10^{20} - 5×10^{23} Pa·s). In Earth, lateral viscosity contrasts are likely to be larger than in our models, and we test the robustness of our base model in a series of 2D simulations with an altered viscosity regime. Furthermore, our model setup does not include plastic yielding.

As in previous studies (e.g., Dannberg & Gassmöller, 2018), we assume an average mantle composition of 82% harzburgite and 18% recycled oceanic crust (Nakagawa et al., 2010; Xu et al., 2008), and compute the material properties ρ, α and Cp using PerpleX (Connolly, 2009) and a

mineral physics database (Stixrude & Lithgow-Bertelloni, 2011). Accordingly, all material properties include the effects of phase transitions, with thermal expansivity and specific heat taking into account the corresponding latent heat release and consumption (Nakagawa et al., 2009).

Our models also account for the anomalously warm material present at the base of the mantle beneath the Pacific and African plates in the present-day Earth (Garnero et al., 2016), with the latter lying below the reconstructed site of the latest supercontinent, Pangea (Torsvik et al., 2006; Burke et al., 2008; Torsvik et al., 2008; 2010; Heron et al., 2021; Murphy et al., 2020). As a result of these present-day temperature anomalies, the mantle's thermal and geoid profiles are characterized by a degree-2 harmonic structure (Zhong et al., 2007). Two regions characterized by low shear wave velocities in seismic tomography (Garnero et al., 2016), and are often referred to as the Large Low Shear Velocity Provinces (LLSVPs) or Large Low Velocity Provinces (LLVPs). There is debate as to whether the LLSVPs' thermal and/or compositional features are chemically distinct from the surrounding mantle (as outlined in McNamara, 2019), and also if these regions are fixed over time (e.g., Torsvik et al., 2010) or able to move with the mantle flow (e.g., Zhang et al., 2010; Zhong & Rudolph, 2015; Flament et al., 2022). In the initial base model, we apply a 200 km dense layer made of mid-ocean ridge basalt (MORB) that is then shaped into hot thermo-chemical piles over the model evolution, similarly to previous studies (Dannberg & Gassmöller, 2018; Heister et al., 2017). The high temperature of these modelled thermochemical structures would reduce seismic velocities, explaining the observation of the LLSVPs. Although the chemical composition of the LLSVPs in the Earth's mantle is unlikely to be basaltic, this composition gives the thermo-chemical piles a buoyancy which facilitates for the formation of stable piles that are dynamic and not entrained into mantle flow. Even though the thermo-chemical pile has a higher density (2% increase) than the ambient mantle (Figure 4), the layer is not fixed in one location and has the potential to move in response to mantle flow generated by subduction (e.g., Zhang et al., 2010; Zhong & Rudolph, 2015; Flament et al., 2022). As a result, we use basaltic material as a rheological proxy for the deep mantle seismic features. The buoyancy number, B, for the thermo-chemical layer can be calculated by $B = \frac{\Delta\rho}{\alpha\rho\Delta T}$. Here Δρ is the density contrast between the anomalously dense material of the thermo-chemical pile and the average mantle composition directly above the layer. In the buoyancy equation, ΔT is the difference between the actual core-mantle boundary temperature (fixed at 3700 K) and the adiabatic profile (at a reference depth of 2500 km). At the core-mantle boundary, the buoyancy number of the thermo-chemical layer is approximately 1.9, where ΔT is 1284 K and the density difference is an increase of 2% (ρ = 5551 kg m^{-3}).

2D model setup

In 2D models, we test different parameters against the generation of plumes following supercontinent formation. Table 3 provides a list of the different models tested, which include running simulations that deviate from the base model in viscosity profile, thermo-chemical pile thickness, and resolution. In order to simulate global-scale tectonic processes, we prescribe plate motions at the surface of the model to re-create a simplified mechanism for the formation of a supercontinent (e.g., a degree-1 mantle flow): (1) we first apply 4 cm/yr of total surface motion convergence (2 cm/yr per side) with an initial large-scale downwelling (subduction) simulating the assembly of plates (Fig 5a), and subsequently (2) the cessation of this initial downwelling is followed by the initiation of subduction zones on the margins of a stationary portion of the surface (i.e.,

circum-supercontinent subduction, Fig 5b-d). Following the cessation of initial subduction, the surface velocity within the model supercontinent is set to zero, while the convergent velocity on its margins remains at 2cm/yr. This two-step process is shown in Figure 5, where three different sizes of the supercontinent are provided (i.e., portions of stationary material covering 20%, 30%, and 40% of the surface). The first step lasts for 400 million years (Myr) in order to allow time for the formation of plumes and slabs from the laterally homogeneous initial condition (e.g., Figure 4).

Following the formation of the model supercontinent, the simulation runs for another 300 Myr (i.e., 700 Myr in total) and the location of a plume arriving at the base of the lithosphere in regions exterior to the supercontinent (i.e., in the oceanic domain) is analysed. Given the timeframe of the formation of the supercontinent Pangea to the present-day is approximately 300 Myr, we have used this temporal range as a cut-off for our simulations. Figure 6 shows the process for analyzing the full 2D simulation, with Figure 6a showing the subduction zone that would bring together a model supercontinent. The overall northward-dipping subduction of the Paleo-Tethys that contributed to Pangea formation is considered as the interior subduction (Figure 1a, Murphy et al., 2009). After 400 Myr, this subduction zone ceases and is replaced by circum-supercontinent subduction around a stationary region covering 30% of the Earth's surface (e.g., Figure 6b). Exterior plume positions forming after supercontinent formation are then calculated using the great circle distance from the edge of the circum-supercontinent subduction zone to the centre of the plume tail (Figures 6c-d). As an example, the base model with a 30% stationary surface generates exterior plumes 3781 km away from the edge of the supercontinent 136 Myr after supercontinent formation (Figure 6c) and 1334 km from the supercontinent edge 249 Myr after supercontinent formation (Figure 6d). The exterior plume timing is manually calculated based on the visual inspection of when the plume head starts to spread out beneath the surface boundary layer (our model lithosphere).

For this study, the simulations and analysis of plumes forming after supercontinent formation (i.e., after the cessation of interior, Paleo-Tethyan analogous subduction) are further split into two categories based on their location. In the simplified 2D simulations, we base this classification on the initial subduction polarity, i.e., the polarity of the angled downwelling (e.g., Figure 1), which also relates to the geographic longitude (i.e., eastern and western hemispheres). In particular, the initial subduction that forms the supercontinent can be split into an overriding and a subducting plate: the western hemisphere of Pangea (Laurentia, Baltica, Siberia, Amazonia) is described as the overriding plate; and the eastern hemisphere is the subducting plate (Figure 1a). In other words, we identify a western and an eastern margin of Pangea, where the Western side corresponds to the North and South American subduction boundary and the Eastern refers to the Australasian subduction zones (Figure 1b). This definition is used to geographically label the overriding and subducting plates in our 2D models (Figure 6) to allow for comparison with Pacific LIPs forming closer to the Australasian (Eastern) or American (Western) subduction zones.

3D model setup

The parameters of the low resolution 2D setup (Model 6) are also applied to a 3D global mantle convection model. The changes between Model 6 and the base model include a reduction in resolution in the bottom 250 km and top 80 km of the model, and the removal of particles to track the compositions within the simulation. The computational time for a 3D spherical model spanning supercontinent formation and dispersal is significant, and therefore the use of particles to track

composition was removed to reduce computational time. However, tests in the 2D setup using this reduced resolution profile did not provide significant changes to the model results (see Figure 10 and 11). As a result of this 2D testing and the computational expense of the global models, we only provide one 3D model here.

The 3D simulation setup is similar to the 2D setup in that an initial formation period is applied with one, interior subduction zone at 4 cm/yr total convergence (Figure 4a). However, in the 3D models this time period is 300 Myr, which is 100 Myr shorter than the 2D simulations in order to save computational time. The goal of this initial formation period in 3D is to provide sufficient time for the mantle to mix from its initial condition. After 300 Myr, the boundary condition at the surface is then provided by global plate reconstructions of Pangean formation and dispersal, rather than the simple 2D setup of a stationary supercontinent. In this study, we use the Matthews et al. (2016) plate reconstructions, which extends back in time 410 million years (i.e., to prior to supercontinent formation) to the present day and thereby encompassing the formation and break-up of Pangea.

We apply the Matthews et al. (2016) surface velocities at 1 Myr intervals, with a resolution of 1° × 1°. As the boundary condition at the surface is provided by plate reconstructions and is therefore kinematic (i.e., it does not change in accordance with the force balance of the underlying mantle), we can show the impact of subduction-driven mantle flow on the positioning of mantle plumes. The 3D simulation is then analysed for plumes in and around the potential sites of the Shatsky Rise (170 Ma), Ontong Java (122 Ma) and the Caribbean (95 Ma) LIPs.

As our study is focused on the impact of subduction on plume generation and applies time-dependent boundary conditions related to plate reconstruction histories to determine mantle flow, we do not need to prescribe continental and oceanic material at the surface as in previous studies (e.g., Coltice et al., 2007, 2009; Phillips et al., 2009; Phillips and Coltice, 2010; Rolf et al., 2012; Yoshida, 2010; Arnould et al., 2020). Although more realistic, the impact of chemically distinct continental material would not be a primary driver of deep mantle plumes (e.g., Heron and Lowman, 2010, 2011, 2014; Heron et al., 2015; Yoshida, 2013) and therefore has not been applied. However, the model uses temperature-dependent viscosity which forms strength differences within the top boundary layer. These are a proxy for the outlines of plates bounded by the ridges and subduction zones produced from the applied plate reconstruction velocities. In that respect, we can generate areas of reduced heat flux due to cold material that thickens in response to plate tectonic processes. As a result, our simulations yield areas of the surface that could be described as a model continent (or interior of a supercontinent) and a model ocean with mid-ocean ridges (exterior of a supercontinent) (Figure 13).

Results

In this section we outline the results from the models shown in Table 3, starting with the 2D simulations.

2D Results

Figure 7 shows the position of the exterior (i.e., sub-superoceanic) plumes for the base model with supercontinent coverage of 20% (Fig. 7a, d), 30% (Fig. 7b, e), and 40% (Fig. 7c, f). In these models, the change in mantle flow due to the formation of the circum-supercontinent downwelling

(subduction) culminates with the production of the first exterior plume near the Eastern boundary for all supercontinent coverage percentages about 140 million years after the final supercontinent formation (i.e., shut-down of interior subduction) (Fig. 7a-c). These Eastern plumes form at approximately 4,400 km (20% coverage, Fig. 7a), 3,700 km (30%, Fig 7b), and 3,800 km (40%, Fig 7c) from the peripheral subduction zone. The Western plumes form later than their Eastern counterparts (Fig. 7d-f), with their distance from the downwelling being more variable (20%: 3,600km; 30%: 1,300 km; 40%: 3,600 km). The delay in the initiation of the plumes may relate to the Western side of the supercontinent being on the overriding plate during supercontinent formation (e.g., Figure 1). Therefore, plume formation beneath the Western margin is suppressed by the cold subducted interior ocean lithosphere covering the core-mantle boundary in that area. In addition, eventual overturn of the subducted slab on the Eastern margin allows for a stronger interaction between the Eastern slab and the sub-superocean thermochemical structure.

The other models performed in this study (Table 3) yield a similar behaviour to the 2D base model (Fig. 7). Figure 8 shows an overview of the timing of the exterior plume arrival plotted against distance from the peripheral subduction zone for both the Eastern and Western regions. Plumes that formed due to the initial condition, and plumes that would have occurred if no supercontinent had formed (e.g., plumes forming due to the initial subduction flow), are not included in our summary. Plumes included in this study are only those related to the new subduction initiation. Eastern plumes typically form before Western plumes, and show a smaller variance in distance from the downwelling. The average timing of the exterior plumes post-supercontinent formation is 157 ± 6 for Eastern plumes (n = 21) and 229 ± 9 Myr for Western plumes (n = 12). The standard deviation for the Eastern and Western ages is 28 Myr and 32 Myr, respectively. The average distance from the subduction for the 2D models was 4,132 ± 221 km for Eastern plumes and 3,252 ± 388 km for Western plumes. The standard deviation for the Eastern and Western locations is 766 km and 1347 km, respectively. The timing cut-off for measuring plumes is set at 300 Myr after supercontinent formation. There are consequently fewer Western plumes during this time-frame due to the delay in plume formation (with plumes forming after the cut-off time of 300 Myr, Figure 7d).

Figure 9 shows the Western plume positions for the different models described in Table 3, for 30 % supercontinent coverage (Model 7 is not shown since no plume(s) formed near the Western margin within 300 Myr of supercontinent formation, but after this cut-off period). As illustrated in Fig. 9, there is variation in the plume positions, with Model 3 (decrease in dense layer thickness, Fig. 9c) and Model 5 (increase in maximum viscosity, Fig. 9e) yielding plumes with the greatest distance from the peripheral subduction zones. Decreasing the resolution in Model 6 (Fig. 9f) produces a similar result to that of Model 1 (Fig. 9a).

Figure 10 shows the Eastern plume position for the different models with 30% coverage, and highlights the summary shown in Figure 8 (earlier plume arrivals and less variance between the distances than Western plumes). The only notable difference between these models is that the decrease in dense material initial thickness in Model 3 (Fig. 10c) produces more vigorous mantle convection. The initially thin dense layer becomes more readily mixed into the mantle, producing more plumes emanating from the core-mantle boundary. However, despite these different dynamics, the plume position for Model 3 forms closest to the Eastern boundary but is similar in timing to the other models (Fig. 11, diamonds).

When changing the continental coverage, no plumes form for the 20% coverage on the Western side during the 700 Myr model run (Figure 12). Furthermore, the 30% continental coverage produces Western plumes at shorter distances from the subduction zone than the 40% coverage (Figure 12). The interaction of the newly formed circum-supercontinent subduction on the Western side either captures a plume beneath the supercontinent (20%), or pushes the thermal instabilities out beneath the exterior on the oceanside (30%, 40%). Conversely, the consistency of the Eastern side results in producing a narrow band of plume timings and distances relates to the absence of subducted lithosphere from the interior ocean, allowing the new circum-supercontinent subduction to disrupt the mantle flow and to form deep thermal instabilities that lead to mantle plumes (regardless of initial model setup, Figure 11-12).

3D Results

Figure 13 shows the evolution of the 3D numerical simulation that prescribes 410 Myr of plate reconstruction history as a time-dependent velocity boundary condition (Matthews et al., 2016). We present snapshots of the thermal structure at a depth of 70 km from the surface, which is sufficiently shallow to resolve the colder continental lithosphere and sufficiently deep to capture any thermal plume arriving beneath the oceanic lithosphere from the core-mantle boundary. The snapshots show the southern Pacific in the left column and the Western boundary of the Americas in the right column, both in the present-day reference frame. Figure 13a-b show the formation of our model Pangea at 300 Ma, bounded by peripheral subduction zones (Figure 1b). We then analyse the models at four key times relating to formation of oceanic LIPs: 170 Ma; 145 Ma (Shatsky Rise), 122 Ma (Ontong Java), and 95 Ma (Caribbean LIP). Figure 14 shows temperature cross-sections that correspond to these four key times.

Figure 13d shows a warm thermal anomaly in the cold lithosphere off the coast of South America at 170 Ma (as highlighted by the white dashed circle). This thermal anomaly can be seen to be related to the arrival of a plume head (Figure 14a). The location of this plume is in the approximate position of the present-day Galapagos hotspot. The plume is also in this location during the timing of the CLIP (Figure 13j and 14d). Our models indicate that the exterior plume activity off the coast of South America is related to circum-supercontinent subduction and occurs at a time-period that links the Galapagos hotspot to the CLIP, as previously discussed in Courtillot & Renne (2003) and Hoernle et al. (2004).

Figure 13e shows the formation of a thermal anomaly in the Pacific at the approximate formation timing and location of the Shatsky Rise (145 Ma). Analysing a thermal cross-section at this time period shows the formation of a plume interacting with a subduction zone situated ~7,200 km away at the Eastern boundary of the Pacific (Figure 14b). Furthermore, the dense anomaly on the core-mantle boundary below the Pacific is clearly visible and shows a plume rising from its margin (Torsvik et al., 2010) despite our thermo-chemical piles being mobile and not fixed in location (Zhang et al., 2010; Zhong & Rudolph, 2015; Flament et al., 2022; Heron et al., 2021). As indicated by the white lines in Figure 14b, we interpret this plume to be an exterior upwelling related to the nearby Eastern subduction.

Figure 13g-h show the Southern Pacific and Western America boundary at 122 Ma and highlights a thermal anomaly arriving near the Antarctica subduction zone. In the cross-section of the mantle's thermal field (Figure 14c), a plume related to this lithospheric anomaly is shown forming along the

southern margin of the dense layer. We interpret this interaction to be due to the exterior return flow related to the Antarctic subduction zone, which occurs at the time of the OJP LIP. Due to the angle of the cross-section, and the 3D nature of the models, it is difficult to show the closeness of the plume and subduction zone. However, the great circle distance between the surface expression of our OJP plume in Fig 13g and 14c and the Antarctica subduction zone is ~4,300 km.

Discussion

Results from our modeling show the impact of modifying global subduction patterns on the location and timing of plumes *exterior* to a supercontinent (Figure 3). Although a number of studies have previously modeled or discussed plume development after supercontinent formation (Biggin et al., 2012; Dannberg & Gassmöller, 2018; Heron et al., 2015; Zhang & Li, 2018; Flament et al., 2017; Sobolev et al. 2011; Dal Zilio et al., 2017), the mechanisms that affect the timing and location of exterior plumes are not well understood. Our study offers a formal analysis of the generation of exterior plumes following supercontinent formation and their relationship to circum-supercontinent subduction (Figure 3). We provide an estimate of the timing and location of such plumes and their variability (Figure 8). Through the 3D simulations, we also visualize this subduction-plume interaction on a global scale. Below we discuss the potential relevance of these findings to the exterior LIPs that remain in the Pacific Ocean contemporarily (Figure 2): the Western LIPs of Ontong Java and Caribbean, and the Eastern LIP Shatsky Rise.

Ontong Java Plateau

The Ontong Java Plateau (OJP) is the world's largest oceanic plateau and is linked to a massive volcanic event that significantly altered global climate and ocean oxygen levels, which was responsible for a mass extinction event (Zhang et al., 2020). The position and geometry of the OJP has changed significantly over time associated with the drifting Pacific plate. The three currently separated plateaux of Ontong Java, Manihiki, and Hikurangi were originally formed in a single complex known as the greater OJP (Chandler et al., 2012; Taylor, 2006). While the greater OJP is thought to have been emplaced by two major magmatic events at about 122 Ma and 90 Ma (Mahoney et al., 1993; Tejada et al., 1996), the cause of the magmatism is still debated (Isse et al., 2021). Two main hypotheses relate OJP formation to a mantle plume (i.e., melting anomalies arising from hot diapirs ascending from the deep mantle: Isse et al., 2021; Tarduno et al., 1991) or to a plate boundary interaction (i.e., melting anomalies fueled by shallow mantle processes associated with plate tectonics: Nakanishi et al., 1999; Frey et al., 2000; Sager et al., 2019).

Although a number of studies have analysed the viability of a mantle plume origin, including studies using seismic evidence (Isse et al., 2021), there is little discussion of the *mechanism* that would have generated the upwelling. The Louisville hotspot, for example, is often discussed as a potential source of the OJP (Tarduno et al., 1991; Chandler et al., 2012), but the mechanism that caused the Louisville plume to form at its specific time and location is not known.

The reconstructed initial emplacement position of the OJP complex is at approximately -38° latitude and 219° longitude (Torsvik et al., 2006; 2008). The closest subduction zone to this region would have been that of Antarctica's western boundary near the South Pole (-75°, 219°), as seen in Figure 1c (Seton, et al., 2012). The distance from the OJP centre to this subduction margin is calculated to be approximately 4,000 km (using a great-circle path). In our 3D model that uses plate

reconstruction velocities to move the surface, we form a plume at 122 Ma and at a distance of ~4,300 km from the Antarctic subduction zone.

To put our 2D models into geological context, we need to modify the OJP emplacement age to a timescale relevant to Pangea formation. The formation of Pangea occurred during the Late Carboniferous period and it is difficult to apply one single age to the formation. However, we assume the cessation of the interior subduction zone that helped form Pangea occurred at ~320 Ma (Pastor-Galán, 2022). We use this single time as a reference in order to create an approximate timing of our plumes to relative to LIP magmatism. The approximate time lag to OJP magmatism following Pangea formation is 198 Myr (320-122 Ma). However, given the uncertainty related to Pangea formation, the timing has an uncertainty in the range of ± 10 Myr. In our 2D models presented above, the Western plumes (which would be most dynamically relatable to the OJP) have an average timing and position (with standard deviation) of 229 ± 32 Myr and 3,252 ± 1,347 km (Fig. 8), which fits well with the observed spatial and temporal range for the OJP.

Caribbean LIP (CLIP)

The Caribbean LIP (CLIP) has a similar chemical composition to the OJP (Hauff et al., 2000), with the main volcanic emplacement occurring between 95 and 88 Ma (Fig 1d). Compared to other LIPs that formed after Pangea formation, CLIP is among the most recent (Torsvik et al., 2006; 2008). Although suggested formation mechanisms for CLIP vary, the Galápagos hotspot has been proposed as a potential deep mantle plume source (Courtillot & Renne, 2003). Our 3D models show the formation of a plume in the approximate location of CLIP from 170 Ma (Figure 13c-d, Figure 14a).

The reconstructed initial emplacement position of CLIP was at approximately 0° latitude and 250° longitude (Scaife et al., 2017). At that time, the closest subduction zone to this was along the western boundary of North and South Americas (0°, 250°), as seen in Fig. 1d (Scaife et al., 2017). The great circle distance from CLIP to this subduction margin is approximately 2,200 km, and, using 320 Ma for the cessation of interior subduction, the age of CLIP with respect to Pangea formation is 225 ± 10 Myr (320-95 Ma). CLIP therefore appears relatively close to the subduction zone, but within the margins of plumes observed in our 2D models, and with a timing that is consistent with our model results (Fig. 8). Our 3D model generates a plume ~1,000 km from the subduction zone of South America and further south of the equator than the CLIP emplacement.

Shatsky Rise

The Shatsky Rise (SR) is the Earth's third largest oceanic plateau (Geldmacher et al., 2014), forming in the exterior to Pangea at approximately 145 Ma (Mahoney et al., 2005). Like the OJP, two main hypotheses exist for the formation of the plateau: a plume origin or plate boundary interaction (seafloor spreading) (Heydolph et al., 2014; Li et al., 2016; Sager et al., 2013; 2019).

The reconstructed initial emplacement position of the Shatsky Rise was at approximately -4° latitude and 219° longitude (Torsvik et al., 2006; 2008). The closest subduction zone to this region would have been in the Eastern Pacific region on the margins of Eurasia (-4°, 150°). The great circle distance from the Shatsky Rise to the subduction margin is therefore nearly 8,000 km. The timing post-Pangea for this LIP is 175 ± 10 Myr and therefore consistent with our 2D results showing earlier Eastern plume formation (Fig 8). While almost all of our 2D models also feature plumes at a similarly

substantial distances from the subduction margin (e.g. Figure 6c,d, Figure 7), they also highlight that this distance is likely too great for the plume to be caused by the direct impact of the circum-supercontinent subduction and it instead may have formed as a natural instability of the thermal boundary layer (which we did not analyse here). However, our 3D models still show a potential interaction with an Eastern subduction zone, producing a mantle return flow and an exterior plume at a distance of ~7,200 km (Figure 14b). For the formation of the Shatsky Rise, Sager et al. (2016) suggests a similar return flow and exterior plume mechanism related to subducted slab and its interaction with the core-mantle boundary, which is demonstrated in our model results.

Uncertainty

The 2D and 3D models presented here are not intended to be a definitive study of the range in the potential timing and location of different oceanic plumes. There are uncertainties in the material properties of the mantle which may affect the calculation of the plume to subduction zone distance, as well as in the timing of the plume head arrival. Moreover, the timings and locations of the real-world examples presented here (OJP, CLIP, and Shatsky Rise) also have uncertainty associated with them. In addition, our 2D models feature stationary subduction zones, which is not realistic when compared to evolution of a typical subduction zone (e.g., Matthews et al., 2016). Although the Western subduction boundary is relatively stationary in a plate tectonic reference frame during the Pangea life span, it is not perfectly stationary as in our 2D models. This is also evidenced by the different timing and location of plumes in our 3D models, where ancient subducted oceanic lithosphere is distributed more widely in the lowermost mantle. However, by using a simplified set of surface boundary conditions we are able to focus on the first-order mechanisms linking supercontinents and plumes.

Despite these uncertainties, our 2D and 3D models are consistent with the timing and location of these three exterior plumes presented here. The findings therefore provide a viable link between the timings and locations of our modelled exterior plumes and observed oceanic plateaux. As such, our study successfully highlights subduction as a potential mechanism for the formation of oceanic LIPs exterior to a supercontinent.

Future work

The modelling presented here proposes a new mechanism explaining the timing and location of exterior plumes in response to supercontinent formation. However, there are still various aspects related to the numerical experiments and geological analyses that would be intriguing to explore further. For example, we present a limited number of 2D numerical experiments and there are a number of key parameters that could be tested expand the breadth of these interpretations. In particular, our subduction zones are static in these 2D models. Trench advance or retreat rate, in addition to the plate convergence rate, would impact the slab morphology and therefore the timing and positioning of these plumes. This may be a factor in the 3D numerical modeling results for the Shatsky Rise, which fall outside the range provided in the 2D simulations (i.e., at a distance >7,000 km). Furthermore, our 2D setup presents a simple model of Pangea formation without any interior subduction. Plate reconstruction history does indicate subduction within the interior of Pangea related to the Paleo-Tethys and Neo-Tethys oceans. An avenue for further exploration would be to determine the potential impact of such events on both interior and exterior plume formation. In addition, including chemically distinct continental lithosphere within the supercontinent area would

be beneficial in creating more realistic subduction dynamics, which could impact the interaction of the subduction zone and the mantle flow. Despite these caveats, however, we maintain that our simplified 2D models provide a primary step in investigating the origin of plumes exterior to the supercontinent.

Although we present models with and without dense piles of material near the base of the mantle, future work could explore the evolution and impact of these piles on long-wavelength mantle convection. In the 2D models presented here, dense piles form under the exterior ocean realm rather than below the supercontinent, which may impact plume formation and timing. In addition, we do not explore the potential impact on our findings of density and geometry of the dee p LLSVP material (and only present the end member cases). Denser and less mobile piles of material could have a control on plume location and plume generation, given their potential impact on the core-mantle heat flow. Furthermore, the impact of changing the initial condition of our numerical models (e.g., temperature profile) would also assist in placing our findings within the context of Earth's secular evolution.

Future work could additionally explore and compare the forces exerted by both exterior and interior plumes on the plates that they impinge on (e.g., Stern, 2007). This might address the role of exterior plumes in supercontinent break-up through far field forces.

Once a further understanding of the mechanisms involved in the formation of plumes from subduction-related mantle flow is achieved (Arnould et al., 2020), it would be possible to characterize all available LIP and hotspot data.

Conclusion

The numerical models presented here show, for the first time, that subduction related to the supercontinent cycle can reproduce the location and timing of exterior (intra-ocean plate) mantle plumes, including those related to the LIPs (or oceanic plateaux) of the Ontong Java, Caribbean, and Shatsky Rise formations (Figure 1, 8, 13, and 14). The results offer insights into the formation of other oceanic LIPs, and suggest that the impact of circum-Pangean subduction zones can extend away from the supercontinent into the mantle beneath the surrounding ocean (Figure 3). This study adds to a body of research that highlights the importance of considering how a supercontinent impacts mantle convection at every stage of the supercontinent cycle.

Acknowledgements

We would like to thank Daniel Pastor-Galán and an anonymous reviewer for their thoughtful comments on this paper.

Author contributions

PH and EG conducted the numerical simulations, GS created the time dependent boundary conditions for the 2D models, AS provided background reading on the subject. All authors contributed to the writing and editing of the manuscript based on their expertise.

Funding

This research was enabled in part by support provided by Compute Ontario (computeontario.ca) and the Digital Research Alliance of Canada (alliancecan.ca) for allocations to PH and RP. We also acknowledge support from a Natural Sciences and Engineering Research Council of Canada Discovery Grants for PH, RP, and JBM. We thank the Computational Infrastructure for Geodynamics (geodynamics.org) which is funded by the National Science Foundation under the awards EAR-2149126, EAR-0949446 and EAR-1550901 for supporting the development of ASPECT. GES acknowledges support from the Research Council of Norway through its Centers of Excellence funding scheme, Project Number 223272, and through its Young Research Talent scheme for "POLARIS - Evolution of the Arctic in Deep Time", Project Number 326238. JD and RG were supported by the NSF grants EAR-2054605 and EAR-1925677.

Data availability

Data and input files related to the numerical modelling of the paper will be made available at https://github.com/heronphi/Heron_Super22. A number of figures in this manuscript were generated using Scientific Colour Maps (Crameri, 2021), the online figure repository s-ink.org (Crameri et al., 2022), and with accessibility in mind (Crameri et al., 2020).

References

Arnould, M., Coltice, N., Flament, N., Mallard, C., 2020. Plate tectonics and mantle controls on plume dynamics. Earth & Planet. Science Lettr. 547,. https://doi.org/10.1016/j.epsl.2020.116439 116439.

Bangerth, W., Dannberg, J., Fraters, M., Gassmoeller, R., Glerum, A., Heister, T., Naliboff, J., 2022a. ASPECT v2.4.0. Zenodo. doi:10.5281/zenodo.6903424

Bangerth, W., Dannberg, J., Fraters, M., Gassmoeller, R., Glerum, A., Heister, T., Naliboff, J., 2022b. ASPECT: Advanced Solver for Problems in Earth's ConvecTion, User Manual. doi:10.6084/m9.figshare.4865333

Beccaluva, L., Bianchini, G., Natali, C., and Siena, F., 2020. Plume-related Paranà-Etendeka igneous province: An evolution from plateau to continental rifting and breakup. Lithos, 362-363, 105484. Retrieved from https://www.sciencedirect.com/science/article/pii/S0024493720301213

Biggin, A. J., Steinberger, B., Aubert, J., Suttie, N., Holme, R., Torsvik, T. H., . . . Hinsbergen, D. J., 2012. Possible links between long-term geomagnetic variations and whole-mantle convection processes. Nature Geoscience, 5, 526-533. doi:10.1038/ngeo1521

Brandl, P.A., Regelous, M., Beier, C., and Haase, K.M., 2013, High mantle temperatures following rifting caused by continental insulation, Nature Geoscience, 6, 391-394, doi: 10.1038/NGEO1758.

Buiter, S.J., Torsvik, T.H., 2014. A review of Wilson Cycle plate margins: A role for mantle plumes in continental break-up along sutures? Gondwana Res. 26 (2), 627–653. https://doi.org/10.1016/j.gr.2014.02.007.

Burke K. & Dewey J.F. 1975. The Wilson Cycle. In: Geological Society of America, Northeastern Section, 10th Annual Meeting, Syracuse, NY, Abstracts with Programs, Boulder, CO, 48.

Burke, K., and J. F. Dewey, 1973, Plume-generated triple junctions: Key indicators in applying plate tectonics to old rocks, J. Geol., 81, 406–433, doi:10.1086/627882.

Burke, K. and Torsvik, T.H., 2004, Derivation of large igneous provinces of the past 200 million years from long-term heterogeneities in the deep mantle, Earth planet. Sci. Lett., 227, 531-538, DOI: 10.1016/j.epsl.2004.09.015.

Burke, K., Steinberger, B., Torsvik, T. H., Smethurst, M. A., 2008, Plume generation zones at the margins of large low shear velocity provinces on the core-mantle boundary. Earth Planet. Sci. Lett., 265, 49-60, DOI: 10.1016/j.epsl.2007.09.042.

Campbell, I.H., and Kerr, A.C. 2007. Editorial: The great plume debate: testing the plume theory. Chemical Geology, 241(3–4): 149–152. doi:10.1016/j.chemgeo.2007.01.013.

Chandler, M., Wessel, P., Taylor, B., Seton, M., Kim, S.-S., & Hyeong, K., 2012. Reconstructing Ontong Java Nui: Implications for Pacific absolute plate motion, hotspot drift and true polar wander.

Earth and Planetary Science Letters, 331-332, 140-151. Retrieved from https://www.sciencedirect.com/science/article/pii/S0012821X12001409

Coffin, M.F., and Eldholm, O. 1994. Large igneous provinces: crustal structure, dimensions, and external consequences. Reviews of Geophysics, 32(1): 1–36. doi:10.1029/93RG02508.

Coltice, N., Phillips, B.R., Bertrand, H., Ricard, Y., and P. Rey, 2007, Global warming of the mantle at the origin of flood basalts over supercontinents, Geology, 35, 391-394, doi: 10.1130/G23240A.1.

Coltice, N., Herve, B., Rey, P., Jourdan, F., Phillips, B.R. and Y. Ricard, 2009, Global warming of the mantle beneath continents back to the Archaean, Gondwana Research, 15, 254-266, DOI: 10.1016/j.gr.2008.10.001.

Condie, K.C., Pisarevsky, S.A., Puetz, S.J., 2021. LIPs, orogens and supercontinents: the ongoing saga. Gondwana Res. 96, 105–121. https://doi.org/10.1016/j.gr.2021.05.002.

Condie, K.C., 2022, Chapter 7 – Earth cycles, Earth as an Evolving Planetary System (Fourth Edition), Academic Press, 197-227, https://doi.org/10.1016/B978-0-12-819914-5.00001-9.

Connolly, J.A.D. 2009. The geodynamic equation of state: What and how. Geochemistry, Geophysics, Geosystems 10, n/a–n/a. URL http://dx.doi.org/10.1029/ 2009GC002540.

Courtillot, V., Jaupart, C., Manighetti, I., Taponier, P., & Besse, J.. 1999. On causal links between flood basalts and continental breakup. Earth and Planetary Science Letters, 166, 177-195, DOI: 10.1016/S0012-821X(98)00282-9.

Courtillot, V. E. & Renne, P. R., 2003, On the ages of flood basalt events. C. R. Geosci. 335, 113–140, DOI: 10.1016/S1631-0713(03)00006-3.

Crameri, F., Shephard, G.E. & Heron, P.J. 2020, The misuse of colour in science communication. Nat Commun 11, 5444 (2020). https://doi.org/10.1038/s41467-020-19160-7

Crameri, F., G.E. Shephard, and E.O. Straume, 2022. Effective high-quality science graphics from s-Ink.org, EarthArXiv, pre-print.

Crameri, F., 2021. Scientific colour maps. Zenodo. doi:10.5281/zenodo.5501399

Crameri, F., Shephard, G. E., & Conrad, C. P. 2019. Plate Tectonics☆. In Reference Module in Earth Systems and Environmental Sciences. Elsevier. doi:https://doi.org/10.1016/B978-0-12-409548-9.12393-0

Dal Zilio, L., Faccenda, M., & Capitanio, F. 2017. The role of deep subduction in supercontinent breakup. Tectonophysics. doi:10.1016/j.tecto.2017.03.006

Dalziel, I.W.D., 1991. Pacific margins of Laurentia and East Antarctica-Australia as a conjugate rift pair: evidence and implications for an Eocambrian supercontinent. Geology, 19, 598-60, DOI: 10.1130/0091-7613(1991)019<0598:PMOLAE>2.3.CO;2.

Dannberg, J., & Gassmöller, R. 2018. Chemical trends in ocean islands explained by plume--slab interaction. Proceedings of the National Academy of Sciences, 115, 4351-4356. doi:10.1073/pnas.1714125115

Davies, D. R., Goes, S., & Sambridge, M. 2015. On the relationship between volcanic hotspot locations, the reconstructed eruption sites of large igneous provinces and deep mantle seismic structure. Earth and Planetary Science Letters, 411, 121-130. doi:10.1016/j.epsl.2014.11.052

Davies, D. R., Goes, S., Davies, J. H., Schuberth, B. S., Bunge, H.-P., & Ritsema, J. 2012. Reconciling dynamic and seismic models of Earth's lower mantle: The dominant role of thermal heterogeneity. Earth and Planetary Science Letters, 353-354, 253-269. doi:10.1016/j.epsl.2012.08.016

Ernst, R.E., 2014. Large Igneous Provinces. Cambridge University Press, 653 p.

Ernst, R. E., K. L. Buchan, I. H. & Campbell, 2005. Frontiers in Large Igneous Province research. Lithos, 79, 271-297, DOI: 10.1016/j.lithos.2004.09.004.

Ernst, R.E. & Bell, K. 2010. Large igneous provinces (LIPs) and carbonatites. Mineralogy and Petrology, 98, 55–76.

Flament, N., Bodur, Ö., Williams, S., & Merdith, A. 2022. Assembly of the basal mantle structure beneath Africa. Nature, 603(7903), 846--851. Retrieved from https://doi.org/10.1038/s41586-022-04538-y

Flament, N., Williams, S., Müller, R. D., Gurnis, M., & Bower, D. J. 2017. Origin and evolution of the deep thermochemical structure beneath Eurasia. Nature Communications, 8, 14164. doi:10.1038/ncomms14164

Foulger, G.R. 2007. The ‘‘plate’’ model for the genesis of melting anomalies. In Plates, plumes, and planetary processes. Edited by G.R. Foulger and D.M. Jurdy. Geological Society of America Special Paper 430, pp. 1–28, doi:10.1130/2007.2430(01).

French, S. W., & Romanowicz, B., 2015. Broad plumes rooted at the base of the Earth's mantle beneath major hotspots. Nature, 525, 95-99. doi:10.1038/nature14876

French, S. W., & Romanowicz, B. A., 2014. Whole-mantle radially anisotropic shear velocity structure from spectral-element waveform tomography. Geophysical Journal International, 199, 1303-1327. doi:10.1093/gji/ggu334

Frey, F. A., Coffin, M. F., Wallace, P. J., Weis, D., Zhao, X., Wise Jr., S. W., Wahnert, V., Teagle, D. A. H., Saccocia, P. J., Reusch, D. N., Pringle, M. S., Nicolaysen, K. E., Neal, C. R., Muller, R. D., Moore, C. L., Mahoney, J. J., Keszthelyi, L., Inokuchi, H., Duncan, R. A., Delius, H., Damuth, J. E., Dam- asceno, D., Coxall, H. K., Borre, M. K., Boehm, F., Barling, J., Arndt, N. T., and Antretter, M., 2000. Origin and evolution of a submarine large igneous province: The Kerguelen Pla- teau and Broken Ridge, southern Indian Ocean. Earth and Planetary Science Letters, 176 (1): 73-89.

Garnero, E. J., McNamara, A. K., & Shim, S.-H., 2016. Continent-sized anomalous zones with low seismic velocity at the base of Earth's mantle. Nature Geoscience, 9, 481-489. doi:10.1038/ngeo2733

Gassmöller, R., Lokavarapu, H., Heien, E., Puckett, E. G., & Bangerth, W., 2018. Flexible and Scalable Particle-in-Cell Methods With Adaptive Mesh Refinement for Geodynamic Computations. Geochemistry, Geophysics, Geosystems, 19, 3596-3604. doi:10.1029/2018GC007508

Geldmacher, J., Van den Bogaard, P., Heydolph, K., and Hoernle, K., 2014. The age of Earth's largest volcano: Tamu Massif on Shatsky Rise (northwest Pacific Ocean). International Journal of Earth Sciences, 103: 2351-2357.

Glišović, P., & Forte, A., 2017. On the deep-mantle origin of the Deccan Traps. Science, 355(6325), 613-616. Retrieved from https://www.science.org/doi/abs/10.1126/science.aah4390

Gurnis, M., Hall, C. & Lavier, L. 2004. Evolving force balance during incipient subduction. Geochemistry, Geophysics, Geosystems, 5, Q07001, https://doi.org/ 10.1029/2003GC000681.

Hastie, W., Watkeys, M., & Aubourg, C., 2014. Magma flow in dyke swarms of the Karoo LIP: Implications for the mantle plume hypothesis. Gondwana Research, 25(2), 736-755. Retrieved from https://www.sciencedirect.com/science/article/pii/S1342937X13002839

Hauff, F., K. Hoernle, G. Tilton, D. Graham, and A. C. Kerr, 2000, Large volume recycling of oceanic lithosphere over short time scales: Geochemical constraints from the Caribbean Large Igneous Province, Earth Planet. Sci. Lett., 174, 247-263.

He, Y., Puckett, E. G., & Billen, M. I., 2017. A discontinuous Galerkin method with a bound preserving limiter for the advection of non-diffusive fields in solid Earth geodynamics. Physics of the Earth and Planetary Interiors, 263, 23-37. doi:10.1016/j.pepi.2016.12.001

Heister, T., Dannberg, J., Gassmöller, R., & Bangerth, W., 2017. High Accuracy Mantle Convection Simulation through Modern Numerical Methods. II: Realistic Models and Problems. Geophysical Journal International, 210, 833-851. doi:10.1093/gji/ggx195

Heron, P. 2019. Mantle plumes and mantle dynamics in the Wilson cycle. Geological Society, London, Special Publications, 470(1), 87-103. Retrieved from https://www.lyellcollection.org/doi/abs/10.1144/SP470-2018-97

Heron, P. J., & Lowman, J. P., 2010. Thermal response of the mantle following the formation of a ``super-plate''. Geophysical Research Letters, 37, n/a--n/a. doi:10.1029/2010gl045136

Heron, P.J. & Lowman, J.P. 2011. The effects of supercontinent size and thermal insulation on the formation of mantle plumes. Tectonophysics, 510, 28–38, https:// doi.org/10.1016/j.tecto.2011.07.002

Heron, P.J. & Lowman, J.P. 2014. The impact of Rayleigh number on assessing the significance of super- continent insulation. Journal of Geophysical Research Solid Earth, 119, 711–733, https://doi.org/10.1002/ 2013JB010484

Heron, P. J., Lowman, J. P., & Stein, C., 2015. Influences on the positioning of mantle plumes following supercontinent formation. Journal of Geophysical Research: Solid Earth, 120, 3628-3648. doi:10.1002/2014jb011727

Heron, P. J., B. Murphy, D. Nance, and R. N. Pysklywec, 2021, Pannotia's mantle signature: the quest for supercontinent identification. In: Murphy, J.B., Strachan, R.A., and Quesada, C., eds. Pannotia To Pangea: Paleozoic orogenic cycles in the circum-North Atlantic region. Geological Society of London Special Publication, https://doi.org/10.1144/SP503-2020-7

Heyn, B. H., Conrad, C. P., & Trønnes, R. G., 2020. How thermochemical piles can (periodically) generate plumes at their edges. Journal of Geophysical Research: Solid Earth, 125(6), e2019JB018726. https://doi.org/10.1029/2019jb018726

Hill, R. I., 1991. Starting plumes and continental break-up, Earth Planet. Sci. Lett., 104, 398–416, doi:10.1016/0012-821X(91)90218-7.

Hoernle, K., Hauff, F., & van den Bogaard, P., 2004. 70 m.y. history (139–69 Ma) for the Caribbean large igneous province. Geology, 32(8), 697–700. https://doi.org/10.1130/G20574.1

Hoffman, P.F., 1991. Did the breakout of Laurentia turn Gondwanaland inside-out? Science, 252, 1409-1412, DOI: 10.1126/science.252.5011.1409.

Hoffman P.F. 1997. Tectonic genealogy of North America. In: Van der Pluijm, B.A. & Marshak, S. (eds) An Introduction to Structural Geology and Tectonics. McGraw-Hill, New York, 459–464.

Isse, T., Suetsugu, D., Ishikawa, A. et al., 2021. Seismic evidence for a thermochemical mantle plume underplating the lithosphere of the Ontong Java Plateau. Commun Earth Environ 2, 98. https://doi.org/10.1038/s43247-021-00169-9

Kronbichler, M., Heister, T., & Bangerth, W., 2012. High Accuracy Mantle Convection Simulation through Modern Numerical Methods. Geophysical Journal International, 191, 12-29. doi:10.1111/j.1365-246X.2012.05609.x

Lay, T., Hernlund, J., Buffett, B.A., 2008. Core–mantle boundary heat flux. Nature Geoscience 1, 25–32.

Lenardic, A., Moresi, L.-N. Jellinek, A. M., and Manga, M., 2005. Continental insulation, mantle cooling, and the surface area of oceans and continents, Earth Planet. Sci. Lett., 234, 317–333, DOI: 10.1016/j.epsl.2005.01.038.

Lenardic, A., Moresi, L.-N. Jellinek, A. M., O'Neill, C., Cooper, C. M., and Lee, C. T., 2011. Continents, supercontinents, mantle thermal mixing, and mantle thermal isolation: Theory, numerical simulations, and laboratory experiments

Li, Z.X. and Zhong, S. 2009. Supercontinent–superplume coupling, true polar wander and plume mobility: plate dominance in whole-mantle tectonics. Physics of the Earth and Planetary Interiors, 176, 143–156, https:// doi.org/10.1016/j.pepi.2009.05.004

Li, Z.-X., Evans, D.A.D., Zhang, S., 2004. A 90◦ Spin on Rodinia: possible causal links between the Neoproterozoic supercontinent, superplume, true polar wander and low latitude glaciation, Earth and Planetary Science Letters, 220, 409-421, DOI: 10.1016/S0012-821X(04)00064-0.

Li, Z.-X., Bogdanova, S.V., Collins, A.S., Davidson, A., De Waele, B., Ernst, R.E., Fitzsimons, I.C.W., Fuck, R.A., Gladkochub, D.P., Jacobs, J., Karlstrom, K.E., Lu, S., Natapov, L.M., Pease, V., Pisarevsky, S.A., Thrane, K., & Vernikovsky, V., 2008. Assembly, configuration, and break-up history of Rodinia: a synthesis. Precambrian Research, 160, 179-210, DOI: 10.1016/j.precamres.2007.04.021.

Li, S. Z., Yu, S., Suo, Y. H., Wu, T. T., Somerville, I., Sager, W., Li, X. Y., Hui, G. G., Zhang, Y., Zang, Y. B., and Zheng, Q. L., 2016. Orientation of joints and arrangement of solid inclusions in fibrous veins in the Shatsky Rise, NW Pacific: Im- plications for crack-seal mechanisms and stress fields. Geo- logical Journal, 51 (S1): 562-578.

Mahoney, J., Duncan, R., Tejada, M., Sager, W., & Bralower, T., 2005. Jurassic-Cretaceous boundary age and mid-ocean-ridge--type mantle source for Shatsky Rise. Geology, 33(3), 185-188. Retrieved from https://doi.org/10.1130/G21378.1

Mahoney, J., Storey, M., Duncan, R., Spencer, K., & Pringle, M. 1993. Geochemistry and Age of the Ontong Java Plateau. 233-261. Retrieved from http://pubs.er.usgs.gov/publication/70187137

Marzoli, A., Callegaro, S., Dal Corso, J., Davies, J., Chiaradia, M., Youbi, N., Jourdan, F., 2018. The Central Atlantic Magmatic Province (CAMP): A Review. In L. Tanner (Ed.), The Late Triassic World: Earth in a Time of Transition (pp. 91--125). Cham: Springer International Publishing. Retrieved from https://doi.org/10.1007/978-3-319-68009-5_4

Matthews, K. J., Maloney, K. T., Zahirovic, S., Williams, S. E., Seton, M., & Müller, R. D., 2016. Global plate boundary evolution and kinematics since the late Paleozoic. Global and Planetary Change, 146, 226-250. doi:https://doi.org/10.1016/j.gloplacha.2016.10.002

McKenzie, D.P. 1977. The initiation of trenches: a finite amplitude instability. In: In: Talwani, M. & Pitman, W.C. III (eds) Island Arcs, Deep Sea Trenches and Back-Arc Basins. American Geophysical Union, Mau- rice Ewing Series, Washington DC, pp. 57–61.

McNamara, A., 2019. A review of large low shear velocity provinces and ultra low velocity zones. Tectonophysics, 760, 199-220. Retrieved from https://www.sciencedirect.com/science/article/pii/S0040195118301586

McNamara, A. K., & Zhong, S., 2005. Thermochemical structures beneath Africa and the Pacific Ocean. Nature, 437, 1136-1139. doi:10.1038/nature04066

Mitchell, R.N, Zhang, N., Salminen, J., Liu, Y., Spencer, C.J, Steinberger, B., Murphy, J.B., Li, Z.-X., 2021. The supercontinent cycle: Linking mantle convection and plate tectonic theory. Nature Reviews Earth & Environment, 2, 358-374. https://doi.org/10.1038/s43017-021-00160-0

Moores, E.M., 1991. Southwest U.S.-East Antarctic (SWEAT) connection: a hypothesis. Geology, 19, 425-428, DOI: 10.1130/0091-7613(1991)019<0425:SUSEAS>2.3.CO;2.

Murphy, J.B., Nance, R.D. , Cawood, P.A., Collins, W.J., Dan, W., Doucet, L., Heron, P.J., Li, Z.-X., Mitchell, R.N., Pisarevsky, S., Pufahl, P., Quesada, C., Spencer, C.J., Strachan, R.A., & Wu, L., 2020. Pannotia: In defence of its existence and geodynamic significance. In: Murphy, J.B., Strachan, R.A., and Quesada, C., eds. Pannotia To Pangea: Paleozoic orogenic cycles in the circum-North Atlantic region. Geological Society of London Special Publication, https://doi.org/10.1144/SP503-2020-96

Murphy, J.B., Nance, R.D., and Cawood, P.A., 2009. Contrasting modes of supercontinent formation and the conundrum of Pangea. Gondwana Research, 15, 408–420.

Murphy, J.B., & Nance, R.D., 1991. A supercontinent model for the contrasting character of Late Proterozoic Orogenic belts. Geology 19, 469–472.

Murphy, J.B., Gutierrez-Alonso, G., Nance, R.D., Fernandez-Suarez, J., Keppie, J.D., Quesada, C., Strachan, R.A., and Dostal, J., 2006. Origin of the Rheic Ocean: rifting along a Neoproterozoic suture? Geology, 34, 325-328.

Nakagawa, T., Tackley, P. J., Deschamps, F., & Connolly, J. A., 2009. Incorporating self-consistently calculated mineral physics into thermochemical mantle convection simulations in a 3-D spherical shell and its influence on seismic anomalies in Earth's mantle. Geochemistry, Geophysics, Geosystems, 10, n/a--n/a. doi:10.1029/2008gc002280

Nakagawa, T., Tackley, P. J., Deschamps, F., & Connolly, J. A., 2010. The influence of MORB and harzburgite composition on thermo-chemical mantle convection in a 3-D spherical shell with self-consistently calculated mineral physics. Earth and Planetary Science Letters, 296, 403-412. doi:10.1016/j.epsl.2010.05.026

Nakanishi, M., Sager, W.W., Klaus, A., 1999. Magnetic lineations within Shatsky Rise,northwest Pacific Ocean: implications for hot spot-triple junction interaction andoceanic plateau formation. Journal of Geophysical Research 104, 7539–7556.

Nance, R.D., Worsley, T.R. & Moody, J.B., 1986. Post-Archean biogeochemical cycles and long-term episodicity in tectonic processes. Geology 14, 514-518.

Nance, R.D. & Murphy, J.B. 2013. Origins of the supercontinent cycle. Geoscience Frontiers, 4, 439–448, https://doi.org/10.1016/j.gsf.2012.12.007

Nomura, R., Hirose, K., Uesugi, K., Ohishi, Y., Tsuchiyama, A., Miyake, A., & Ueno, Y., 2014. Low Core-Mantle Boundary Temperature Inferred from the Solidus of Pyrolite. Science, 343, 522-525. doi:10.1126/science.1248186

O'Neill, C. J., & Zhang, S., 2018. Lateral Mixing Processes in the Hadean. Journal of Geophysical Research: Solid Earth, 123, 7074-7089. doi:https://doi.org/10.1029/2018JB015698

Pastor-Galán, D., Nance, R.D., Murphy, J.B., & Spencer, C.J., 2019. Supercontinents: myths, mysteries and milestones, In: Wilson, R. W., Houseman, G. A., McCaffrey, K. J. W., Doré, A. G. & Buiter, S. J. H. (eds) Fifty Years of the Wilson Cycle Concept in Plate Tectonics. Geological Society, London, Special Publication 470, 39-64.

Pastor-Galán, D. 2022. From supercontinent to superplate: Late Paleozoic Pangea's inner deformation suggests it was a short-lived superplate. Earth-Science Reviews, 226, 103918.

Phillips, B.R., Bunge, H.P. & Schaber, K. 2009. True polar wander in mantle convection models with multiple, mobile continents: Gondwana Research, 15, 288–296, http://doi.org/10.1016/j.gr.2008.11.007

Phillips, B.R. & Coltice, N. 2010. Temperature beneath continents as a function of continental cover and convective wavelength. Journal of Geophysical Research, 115, B04408, https://doi.org/10.1029/2009 JB006600

Rainbird, R.H., and Ernst, R.E. 2001. The sedimentary record of mantle-plume uplift. In Mantle plumes: their identification through time. Edited by R.E. Ernst and K.L. Buchan. Geological Society of America, Special Paper 352, pp. 227–245, doi: 10.1086/648225.

Rolf, T., Coltice, N. & Tackley, P.J. 2012. Linking continental drift, plate tectonics and the thermal state of the Earth's mantle. Earth and Planetary Science Letters, 351–352, 134–146, https://doi.org/10.1016/j.epsl. 2012.07.011

Sager, W. W., Huang, Y., Tominaga, M., Greene, J., Nakanishi, M., and Zhang, J., 2019. Oceanic plateau formation by sea- floor spreading implied by Tamu Massif magnetic anomalies. Nature Geoscience, 12: 661-666.

Sager, W. W., Sano, T., & Geldmacher, J., 2016. Formation and evolution of Shatsky Rise oceanic plateau: Insights from IODP Expedition 324 and recent geophysical cruises. Earth-Science Reviews, 159, 306–336. https://doi.org/10.1016/j.earscirev.2016.05.011

Sager, W.W., Zhang, J., Korenaga, J., Sano, T., Koppers, A.A.P., Widdowson, M., Mahoney, J.J., 2013. An immense shield volcano within the Shatsky Rise oceanic plateau, northwest Pacific Ocean. Nature Geoscience 6, 976–981.

Saunders, A.D., Jones, S.M., Morgan, L.A., Pierce, K.L., Widdowson, M., and Xu, Y.G. 2007. Regional uplift associated with continental large igneous provinces: the roles of mantle plumes and the lithosphere. Chemical Geology, 241(3–4): 282–318. doi:10.1016/j.chemgeo.2007.01.017.

Scaife, J. D., Ruhl, M., Dickson, A. J., Mather, T. A., Jenkyns, H. C., Percival, L. M., Minisini, D., 2017. Sedimentary Mercury Enrichments as a Marker for Submarine Large Igneous Province Volcanism? Evidence From the Mid-Cenomanian Event and Oceanic Anoxic Event 2 (Late Cretaceous). Geochemistry, Geophysics, Geosystems, 18, 4253-4275. doi:https://doi.org/10.1002/2017GC007153

Sengör, A.M.C. 2001. Elevation as indicator of mantle-plume activity. In Mantle plumes: their identification through time. Edi- ted by R.E. Ernst and K.L. Buchan. Geological Society of America, Special Paper 352, pp. 183–225, DOI: 10.1130/0-8137-2352-3.183.

Seton, M., Müller, R. D., Zahirovic, S., Gaina, C., Torsvik, T., Shephard, G., Chandler, M., 2012. Global continental and ocean basin reconstructions since 200Ma. Earth-Science Reviews, 113, 212-270. doi:https://doi.org/10.1016/j.earscirev.2012.03.002

Sleep, N.H. 1990. Hotspots and mantle plumes: some phenomenology. Journal of Geophysical Research, 95(B5): 6715–6736. doi:10.1029/JB095iB05p06715.

Sobolev, S. V., Sobolev, A. V., Kuzmin, D. V., Krivolutskaya, N. A., Petrunin, A. G., Arndt, N. T., Vasiliev, Y. R. 2011. Linking mantle plumes, large igneous provinces and environmental catastrophes. Nature, 477, 312-316. doi:10.1038/nature10385

Sobolev A. V., Hofmann A. W., Kuzmin D. V., Yaxley G. M., Arndt N. T., Chung S. L., Danyushevsky L. V., Elliott T., Frey F. A., Garcia M. O., Gurenko A. A., Kamenetsky V. S., Kerr A. C., Krivolutskaya N. A., Matvienkov V. V., Nikogosian I. K., Rocholl A., Sigurdsson I. A., Sushchevskaya N. M. and Teklay M. 2007. The amount of recycled crust in sources of mantle-derived melts. Science 316, 412–417.

Steinberger, B., & Calderwood, A. R., 2006. Models of large-scale viscous flow in the Earth's mantle with constraints from mineral physics and surface observations. Geophysical Journal International, 167, 1461-1481. doi:10.1111/j.1365-246x.2006.03131.x

Stern R J. 2007. When and how did plate tectonics begin? Theoretical and empirical considerations. Chin Sci Bull, 52: 578–591

Stixrude, L., & Lithgow-Bertelloni, C., 2011. Thermodynamics of mantle minerals - II. Phase equilibria. Geophysical Journal International, 184, 1180-1213. doi:10.1111/j.1365-246x.2010.04890.x

Straume, E. O., Gaina, C., Medvedev, S., Hochmuth, K., Gohl, K., Whittaker, J. M., et al., 2019. GlobSed: Updated total sediment thickness in the world's oceans. Geochemistry, Geophysics, Geosystems, 20, 1756– 1772. https://doi.org/10.1029/2018GC008115

Svensen, H.H., Torsvik, T., Callegaro, S., Augland, L., Hatlen Heimdal, T., Jerram, D., Planke, S., Pereira, E., 2017. Gondwana Large Igneous Provinces: Plate reconstructions, volcanic basins and sill volumes. Geol. Soc., London, Spec. Publ. 463. SP463.7. 10.1144/SP463.7.

Tan, E., Gurnis, M., & Han, L., 2002. Slabs in the lower mantle and their modulation of plume formation. Geochemistry, Geophysics, Geosystems 3, 1067. doi:10.1067/ 2001GC000238.

Tarduno, J.A., Sliter, W.V., Kroenke, L.W., Leckie, M., Mahoney, J.J., Musgrave, R.J., Storey,M., Winterer, E.L., 1991. Rapid formation of the Ontong Java Plateau by Aptian mantle plume volcanism. Science 254, 399–403.

Taylor, B. 2006. The single largest oceanic plateau: Ontong Java--Manihiki--Hikurangi. Earth and Planetary Science Letters, 241(3), 372-380. Retrieved from https://www.sciencedirect.com/science/article/pii/S0012821X05008356

Tejada, M. L., Mahoney, J. J., Duncan, R. A., & Hawkins, M. P., 1996. Age and Geochemistry of Basement and Alkalic Rocks of Malaita and Santa Isabel, Solomon Islands, Southern Margin of Ontong Java Plateau. Journal of Petrology, 37(2), 361-394. Retrieved from https://doi.org/10.1093/petrology/37.2.361

Torsvik, T. H., & Cocks, L. R. M., 2016. Tectonic units of the Earth. In L. R. M. Cocks & T. H. Torsvik (Eds.),Earth history and palaeo-geography(pp. 38–76). Cambridge, UK: Cambridge University Press.

Torsvik, T., 2003. The Rodinia jigsaw puzzle. Science 300, 1379–1381, doi: DOI: 10.1126/science.1083469.

Torsvik, T.H., Smethurst, M.A., Burke, K. and Steinberger, B., 2006, Large igneous provinces generated from the margins of the large low-velocity provinces in the deep mantle. Geophys. J. Int., 167, 1447- 1460, doi: 10.1111/j.1365-246X.2006.03158.x.

Torsvik, T.H., Steinberger, B., Cocks, R. M., and Burke, K., 2008, Longitude: Linking Earth's ancient surface to its deep interior, Earth and Planetary Science Letters, 276, 273282, https://doi.org/10.1016/j.epsl.2008.09.026.

Torsvik, T.H., Burke, K., Steinberger, B., Webb, S.J., and Ashwal, L.D., 2010, Diamonds sampled by plumes from the core-mantle boundary, Nature, 466, doi:10.1038/nature09216.

White, W. 1985. Sources of oceanic basalts: Radiogenic isotopic evidence. Geology, 13(2), 115-118. Retrieved from https://doi.org/10.1130/0091-7613(1985)13%3C115:SOOBRI%3E2.0.CO;2

White, R., & McKenzie, D., 1989. Magmatism at rift zones: the generation of volcanic continental margins and flood basalts. Journal of Geophysical Research, 94, 7685–7729.

Wilson, J.T. 1966. Did the Atlantic close and then re-open? Nature, 211, 676–681, https://doi.org/10.1038/ 211676a0

Williams, C. D., Mukhopadhyay, S., Rudolph, M. L., & Romanowicz, B., 2019. Primitive helium is sourced from seismically slow regions in the lowermost mantle. Geochemistry, Geophysics, Geosystems, 20, 4130–4145. https://doi.org/10.1029/2019GC008437

Worsley, T.R., Nance, R.D., Moody, J.B. 1984. Global tectonics and eustasy for the past 2 billion years. Marine Geology 58, 373-400, DOI: 10.1016/0025-3227(84)90209-3.

Xu, W., Lithgow-Bertelloni, C., Stixrude, L., & Ritsema, J., 2008. The effect of bulk composition and temperature on mantle seismic structure. Earth and Planetary Science Letters, 275, 70-79. doi:10.1016/j.epsl.2008.08.012

Yale, L. B., and Carpenter, S. J., 1998, Large igneous provinces and giant dike swarms: proxies for supercontinent cyclicity and mantle convection, Earth and Planetary Science Letters, 163, 109-122, https://doi.org/10.1016/S0012-821X(98)00179-4.

Yoshida, M. 2010. Preliminary three-dimensional model of mantle convection with deformable, mobile continental lithosphere. Earth and Planetary Science Letters, 295, 205–218, https://doi.org/10.1016/j.epsl. 2010.04.001

Yoshida, M. 2013. Mantle temperature under drifting deformable continents during the supercontinent cycle. Geophysical Research Letters, 40, 1–6, https:// doi.org/10.1002/grl.50151

Zhang, J., Luo, Y. & Chen, J. 2020. Oceanic Plateau Formation Implied by Ontong Java Plateau, Kerguelen Plateau and Shatsky Rise. J. Ocean Univ. China 19, 351–360. https://doi.org/10.1007/s11802-020-4246-2

Zhang, N., S. Zhong, W. Leng, and Z.-X. Li, 2010. A model for the evolution of the Earth's mantle structure since the Early Paleozoic, J. Geophys. Res., 115, B06401, doi:10.1029/2009JB006896.

Zhang, N., & Li, Z.-X., 2018. Formation of mantle ``lone plumes'' in the global downwelling zone --- A multiscale modelling of subduction-controlled plume generation beneath the South China Sea. Tectonophysics, 723, 1-13. doi:https://doi.org/10.1016/j.tecto.2017.11.038

Zhong, S. J., Zhang, N., Li, Z. X., & Roberts, J., 2007. Supercontinent cycles, true polar wander, and very long wavelength mantle convection. Earth and Planet. Sci. Lett., 375. doi:https://doi.org/10.1016/j.epsl.2007.07.049

Zhong, S., and M. L. Rudolph 2015, On the temporal evolution of long- wavelength mantle structure of the Earth since the early Paleozoic, Geochem. Geophys. Geosyst., 16, 1599– 1615, doi:10.1002/2015GC005782.

Figure Captions

Figure 1: *A global plate tectonic reconstruction* (Matthews et al., 2016) *illustrating the different stages of the supercontinent cycle (left) with schematic mantle processes (right). Blue lines identify ancient oceanic ridges and red lines with teeth locate ancient subduction zones. Present-day continental interior is shown in grey. a) Subduction related to Pangea supercontinent formation at 335 Ma (with final interior subduction zone highlighted by purple lines); b) Circum-supercontinent subduction during Pangea tenure at 300 Ma (with Eastern and Western sides labelled); c-d) Approximate plate tectonic configurations at the time of the major large igneous province formation in (c) the early Cretaceous* (Seton et al., 2012) *and (d) of the Caribbean LIP formation* (Scaife et al., 2017)*, as shown by orange markers. Abbreviations: CAMP: Central Atlantic Magmatic Province; OJP: Ontong Java Plateau; KR: Karoo Ridge; BU: Bunbury Basalts; CLIP: Caribbean large igneous province; SR: Shatsky Rise.*

Figure 2: *Age of the oceanic lithosphere, from Straume et al. (2019), with superposed oceanic Large Igneous Provinces (LIPs) from Torsvik & Cocks (2016) coloured in light blue. NAIP: North Atlantic Igneous Province, HALIP: High Arctic Large Igneous Province. This graphic by Eivind O. Straume from Straume et al. (2019) is available via the open-access s-Ink repository.*

Figure 3: *The subducting oceanic plate influencing interior and exterior plumes as part of whole-mantle convection system. Illustrative cartoon showing the potential process by which a sinking plate could produce return flow in the form of hot mantle plumes both the interior continental region and in the exterior oceanic region (e.g., generating LIPs in the subducting plate).*

Figure 4: *Initial condition setup for the 2D base model. a) Temperature profile from 3700 K at base of model to 273K at surface; b) initial viscosity profile ranging from 1×10^{20} to 5×10^{23} Pa·s; c) initial deep layer (e.g., a dense LLSVP layer) at base of model; d) initial resolution profile showing higher resolution at the base of the model and in the upper mantle and lithosphere; e) initial viscosity profile from the surface (0 km depth) to the core-mantle boundary; f) initial temperature profile.*

Figure 5: *Schematic of the two-step process for modelling supercontinent formation in 2D. (a) The initial subduction zone simulations convergent surface motion. (b-d) Surface motion is such that a portion of the surface is stationary (b: 20%; c: 30%; d: 40%), with two convergent boundaries forming on the margins of the stationary area (i.e., circum-supercontinent subduction). CMB: Core-mantle boundary.*

Figure 6: *Summary of the base model results. a) Initial downwelling zone which models subduction bringing continents together (e.g., Figure 5a). Black arrows indicate convergent surface velocities of 2 cm/yr for all times and locations (4 cm/yr in total convergence). b) Formation of subduction zones on the margins of a stationary portion of the lithosphere (e.g., model supercontinent covering 30% of the surface). The model here shows results at 100 Myr after the cessation of the initial large-scale downwelling shown in (a). c) Formation of a plume beneath the exterior ocean (i.e., external to the model supercontinent) due to the repositioning of downwelling 136 Myr after cessation of initial downwelling shown in 6a. The distance from downwelling to plume is 3781 km. d) Formation of a plume in the exterior region due to the repositioning of downwelling 249 Myr after cessation of initial downwelling shown in 6a. Panel shows distance from downwelling to plume to be 1334 km. Eastern and Western 'sides' of the circum-supercontinent subduction are denoted as outlined in Figure 1.*

Figure 7: *Base model exterior plume positions for supercontinent coverage of 20% (a, d), 30% (b, e), and 40% (c, f) of the surface. These snapshots capture the moment a deep mantle plume arrives at the base of the lithosphere after the formation of a supercontinent at 400 Myr. The top panels (a-c) show the plume positions related to the Eastern subduction zone of the supercontinent (e.g., Figure 6), and the bottom panels (d-f) relate to the Western subduction zone of the supercontinent (e.g., Figure 6).*

Figure 8: *Overview of the 2D model results, showing plume timing after supercontinent formation plotted against great circle surface distance between the plume and the circum-supercontinent subduction zone for both Eastern (red) and Western (blue) regions. Eastern plumes have an average timing and position of 156 ± 28 Myr and 4,132 ± 766 km. Western plumes have an average timing and position of 229 ± 32 Myr and 3,252 ± 1,347 km (with standard deviation given here and shown by error bars). Approximate positions for plumes related to Ontong Java Plateau (OJP) (black circle), Caribbean LIP (CLIP) (grey circle) and Shatsky Rise (white circle) are shown. Additional breakdown of these results by model and continental coverage type can be found in Figures 11-12.*

Figure 9: *Exterior Western plume positions for supercontinent coverage of 30% for (a) Model 1, (b) Model 2 (increase in thickness of deep layer), (c) Model 3 (decrease in thickness of deep layer), (d) Model 4 (decrease of minimum viscosity), (e) Model 5 (increase of maximum viscosity), and (f) Model 6 (lower resolution). Table 3 describes the differences between the models.*

Figure 10: *Exterior Eastern plume positions for supercontinent coverage of 30% for (a) Model 7 (higher resolution), (b) Model 2 (deep layer increase), (c) Model 3 (deep layer decrease), (d) Model 4 (minimum viscosity decrease), (e) Model 5 (maximum viscosity increase), (f) and Model 6 (lower resolution). Table 3 describes the differences between the models.*

Figure 11: *Overview of the 2D model results, showing surface plume arrival timing after supercontinent formation plotted against plume distance from circum-supercontinent subduction zone for both Eastern (red) and Western (blue) regions. Approximate positions for plumes related to Ontong Java Plateau (black) and the Caribbean LIP (grey) are shown. Model results shown as: Model 1 circles; Model 2 (deep layer increase) squares; Model 3 (deep layer decrease) diamonds; Model 4 (minimum viscosity decrease) crosses; Model 5 (maximum viscosity increase) pluses; Model 6 (lower resolution) hexagrams; and Model 7 (higher resolution) asterisks.*

Figure 12: *Overview of the 2D model results, showing plume timing after supercontinent formation plotted against plume distance from circum-supercontinent subduction zone for both Eastern (red) and Western (blue) regions. Approximate positions for plumes related to Ontong Java Plateau (OJP) and the Caribbean LIP (CLIP) are shown. Model results are split into the different supercontinent coverage values: 20%: circles; 30%: squares; 40%: diamonds.*

Figure 13: *Temperature snapshots of the 3D model result at 70 km depth with a view of the Southern Pacific (left) and the North and South America margin (right). Temperature field is captured (a-b) 300 Ma during Pangean tenure; (c-d) 170 Ma at a time when an upwelling forms off the coast of South America; (e-f) 145 Ma during the approximate timeframe of the Shatsky Rise LIP; (g-h) 122 Ma during the approximate timing of OJP (Ontong-Java Plateau) LIP; and (i-j) 95 Ma during the approximate timing of the Caribbean LIP. White lines indicate cross-sections in Figure 14. Abbreviation CAMP in (d) refers to the Central Atlantic Magmatic Province LIP.*

Figure 14: *Temperature cross-sections of corresponding lines in Figure 13. Panel (a) shows the cross-section (Fig. 13d) relating to the formation of a plume off the coast of South America (170 Ma), which is close to the location of the present-day Galapagos hotspot. Panel (b) shows the cross-section (Fig. 13e) relating to the formation of a plume in the mid-Pacific (145 Ma), which has the approximate location and timing of the Shatsky Rise LIP. Panel (c) shows the cross-section (Fig. 13g) relating to the formation of a plume in the South Pacific (142 Ma), which has the approximate location and timing of the OJP LIP. Panel (d) shows the cross-section (Fig. 13j) relating to timing and location of the Caribbean LIP (CLIP), which in our models has been established since 170 Ma and is in the location of the Galapagos hotspot as shown in (a). White lines indicate mantle return flow to the exterior of the supercontinent.*

Table Captions

Table 1: *Compilation of selected global large igneous provinces (LIPs) contemporaneous to Pangean formation (past 320 Ma) ordered by decreasing age. Those mentioned in this study are indicated in bold. Main emplacement ages are given rather than an emplacement age range, with uncertainty in timing being highly variable across the different LIPs. Data compiled from Torsvik et al., 2006 and Svensen et al., 2018, and references therein.*

Table 2: *Model material parameters. (Steinberger & Calderwood, 2006)* [a]*; (Connolly, 2009; Xu et al., 2008; Stixrude & Lithgow-Bertelloni, 2011)* [b]

Table 3: *List of different suites of 2D models. Each model has a 20%, 30% and 40% supercontinent simulation.*

LIP Name	Main Emplacement Age (Ma)
Interior to Pangea (continental or oceanic)	
Panjal Traps	285
Siberian Traps	251
Central Atlantic (CAMP)	201
Karoo	182
Argo	155
Paran-Etendeka	134
High Arctic (HALIP)	121
Rajhmahal Traps	118
Madagascar	87
Sierra Leone	73
Deccan Traps	65
North Atlantic	61
Ethiopia and Afar	31
Columbia River	15
Peripheral/interior to Pangea (Indian or Southern Ocean; oceanic)	
Bunbury	132
Maud Rise	125
Wallaby Plateau	124
Southern and Central Kerguelen	114, 100
Broken Ridge	95
Peripheral/exterior to Pangea (Pacific Ocean; oceanic)	
Shatsky Rise	**147**
Magellan Rise	145
Greater Ontong-Java (including Hikurangi and Manihiki)	**121, 123, 90**
Nauru	111
Agulhas Plateau	100
Hess Rise	99
Caribbean (CLIP)	**95**

Table 1

Symbol	Variable	Value
η	Dynamic viscosity	1×10^{20} - 5×10^{23} Pa·s [a]
ρ	Density	3.3 – 5.8 g·cm^{-3} (PerpleX[b])
g	Gravitational acceleration	9.81 m·s^{-2}
C_p	Specific heat capacity	1058 - 1250 J kg^{-1} K^{-1} (PerpleX[b])
k	Thermal conductivity	4.7 W·m^{-1}·K^{-1}
H	Radiogenic heat production	6×10^{-12} W·kg^{-1}
α	Thermal expansivity	0.65 – 3.6×10^{-5} K^{-1} (PerpleX[b])
E	Activation energy	300 and 800 kJ mol^{-1} [a]

Table 2

Model	Change to base model	Detail
1	Base model	(see Table 2)
2	Increase in deep layer thickness	Increase from 200 km initial thickness to 300 km
3	Decrease in deep layer thickness	Reduction from 200 km initial thickness to 100 km (resulting in entrainment into mantle)
4	Decrease of minimum viscosity	Reduced to 10^{19} Pa·s from 10^{20} Pa·s
5	Increase of maximum viscosity	Increased to 10^{24} Pa·s from 5×10^{23} Pa·s
6 and 3D	Resolution decrease from base model (low). Applied to 3D models.	Decreased refinement in the bottom 250 km and top 80 km of the model (refinement level 6) and removal of particles as a compositional field tracer.
7	Resolution increase from base model (high)	Initial global mesh refinement increased from level 5 to 6, with increased refinement in the bottom 250 km and top 80 km of the model (refinement level 8)

Table 3

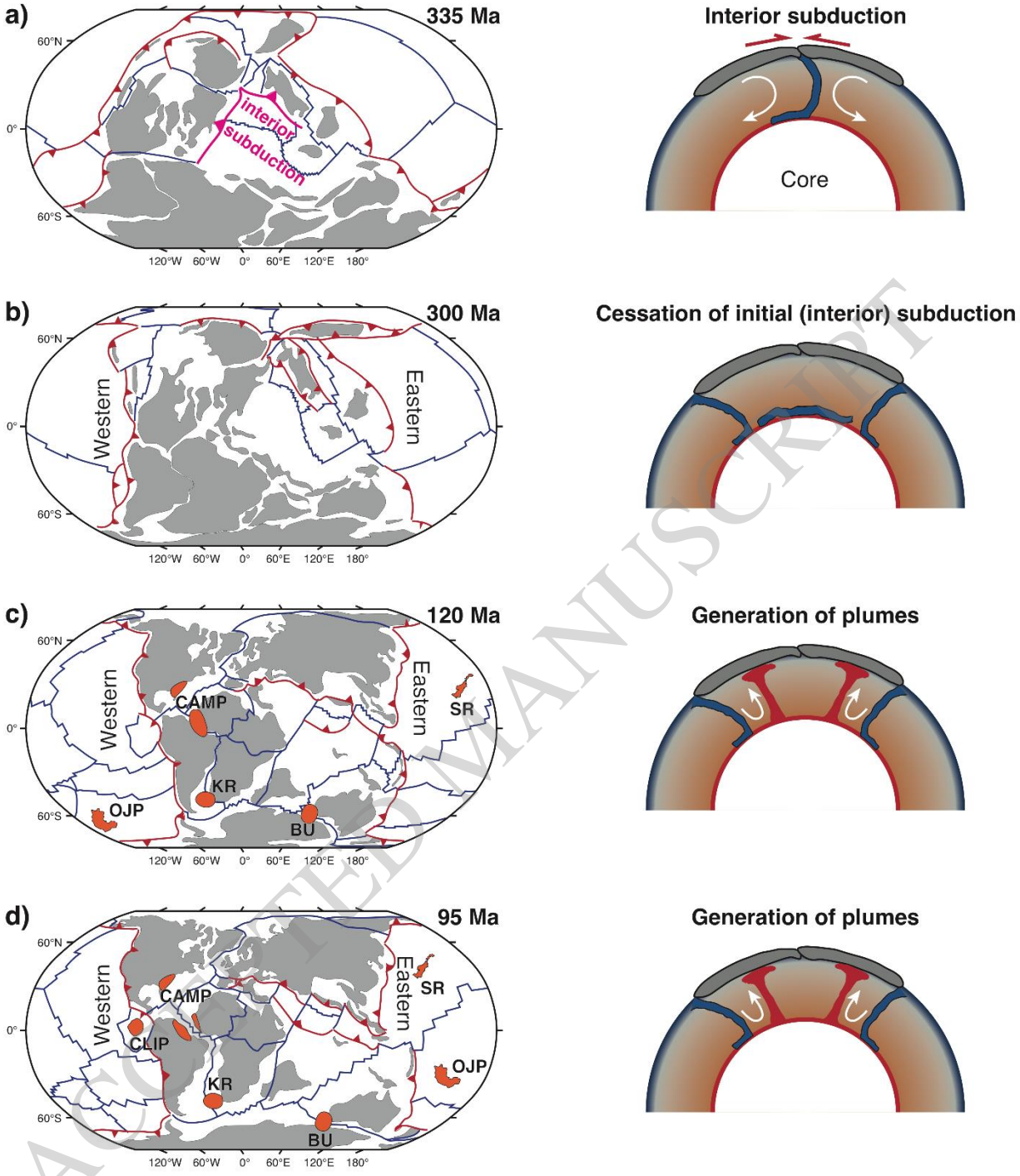

Figure 1

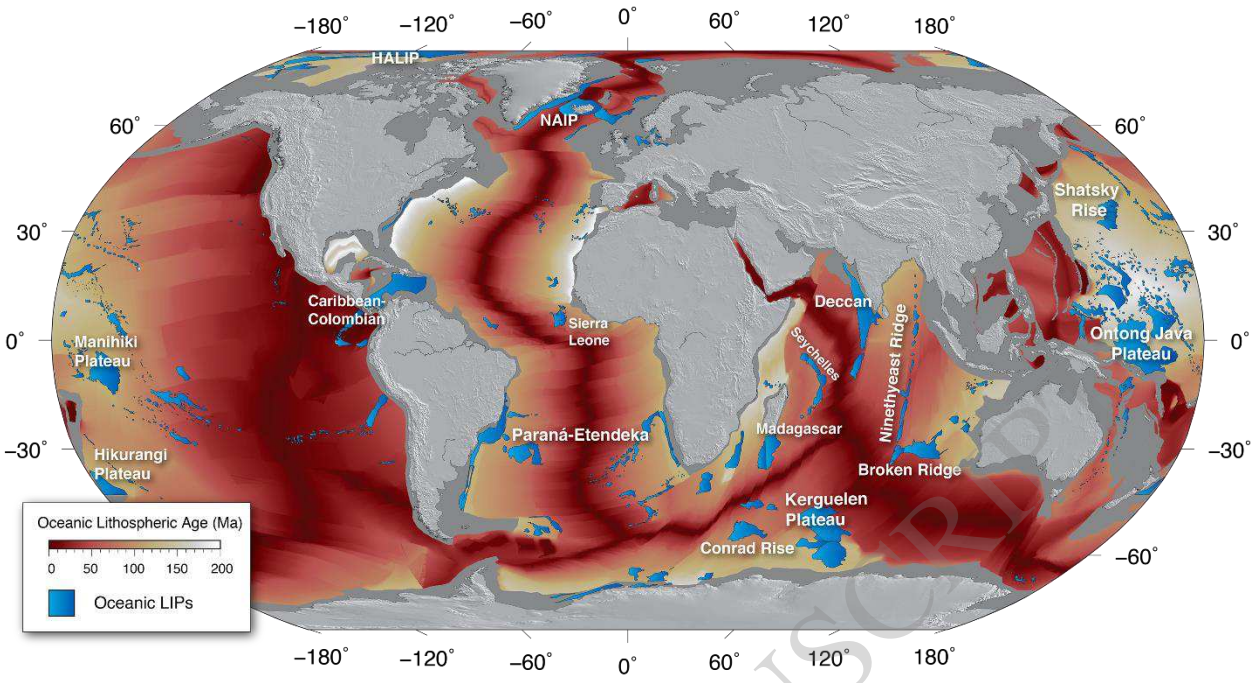

Figure 2

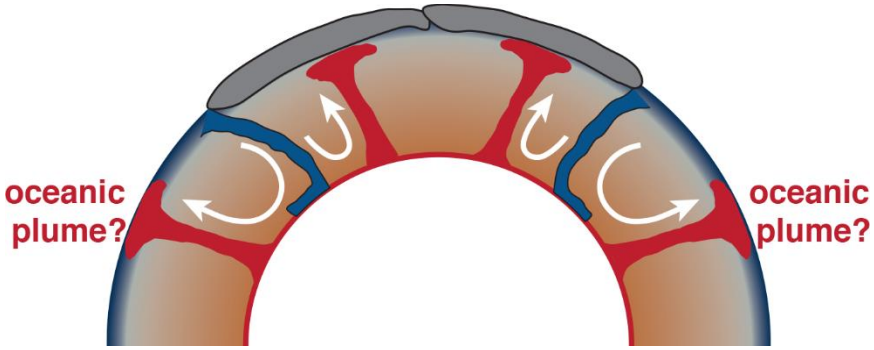

Figure 3

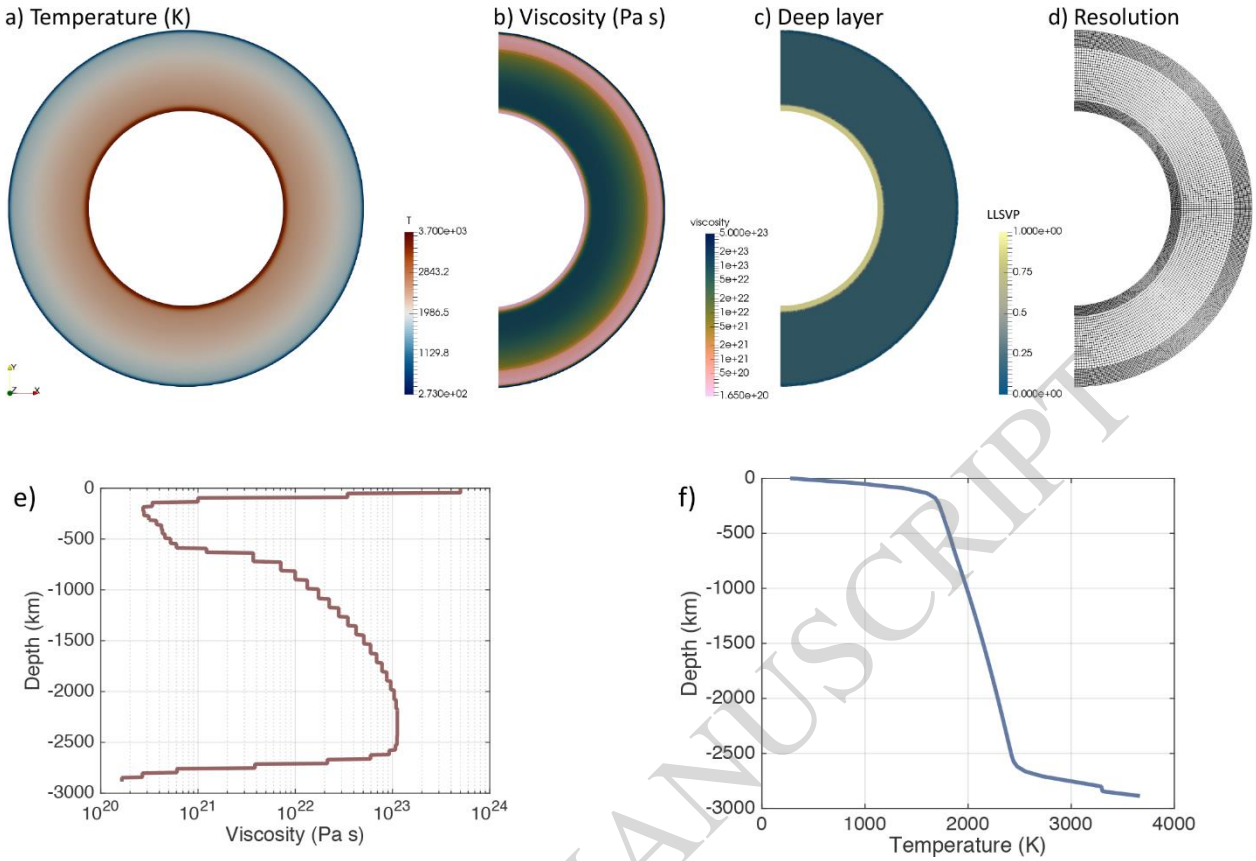

Figure 4

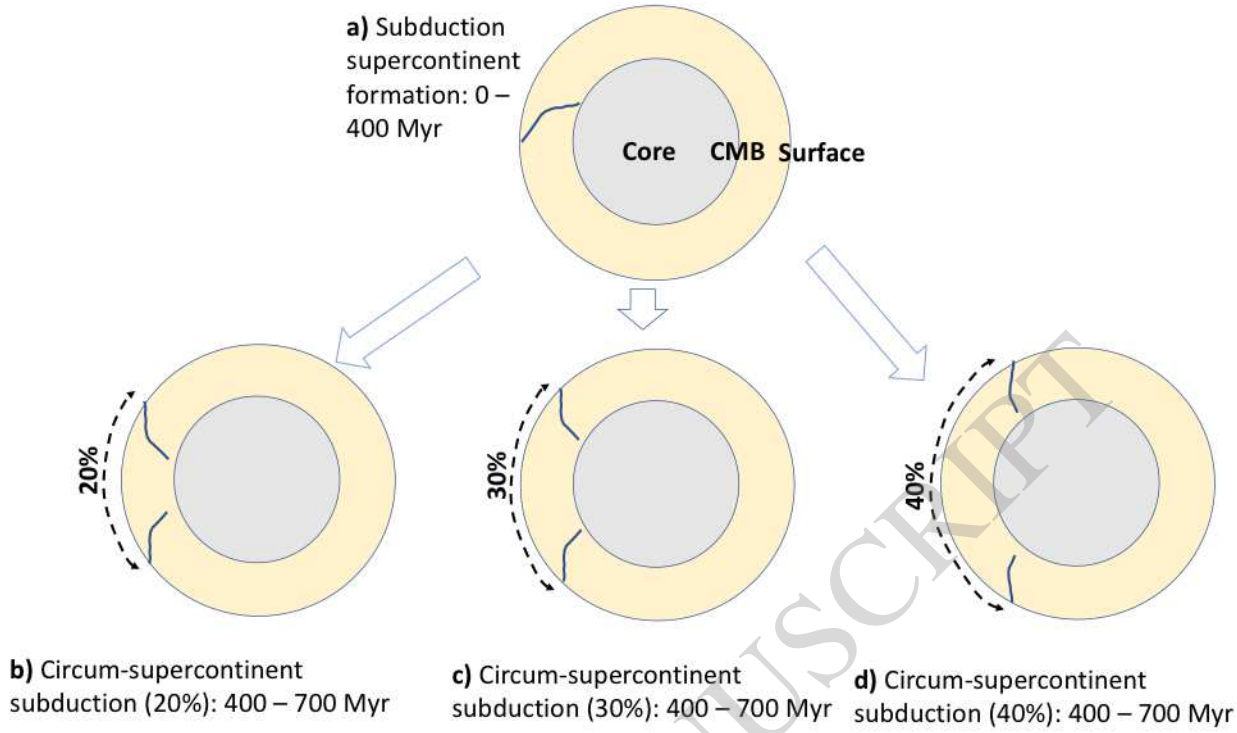

Figure 5

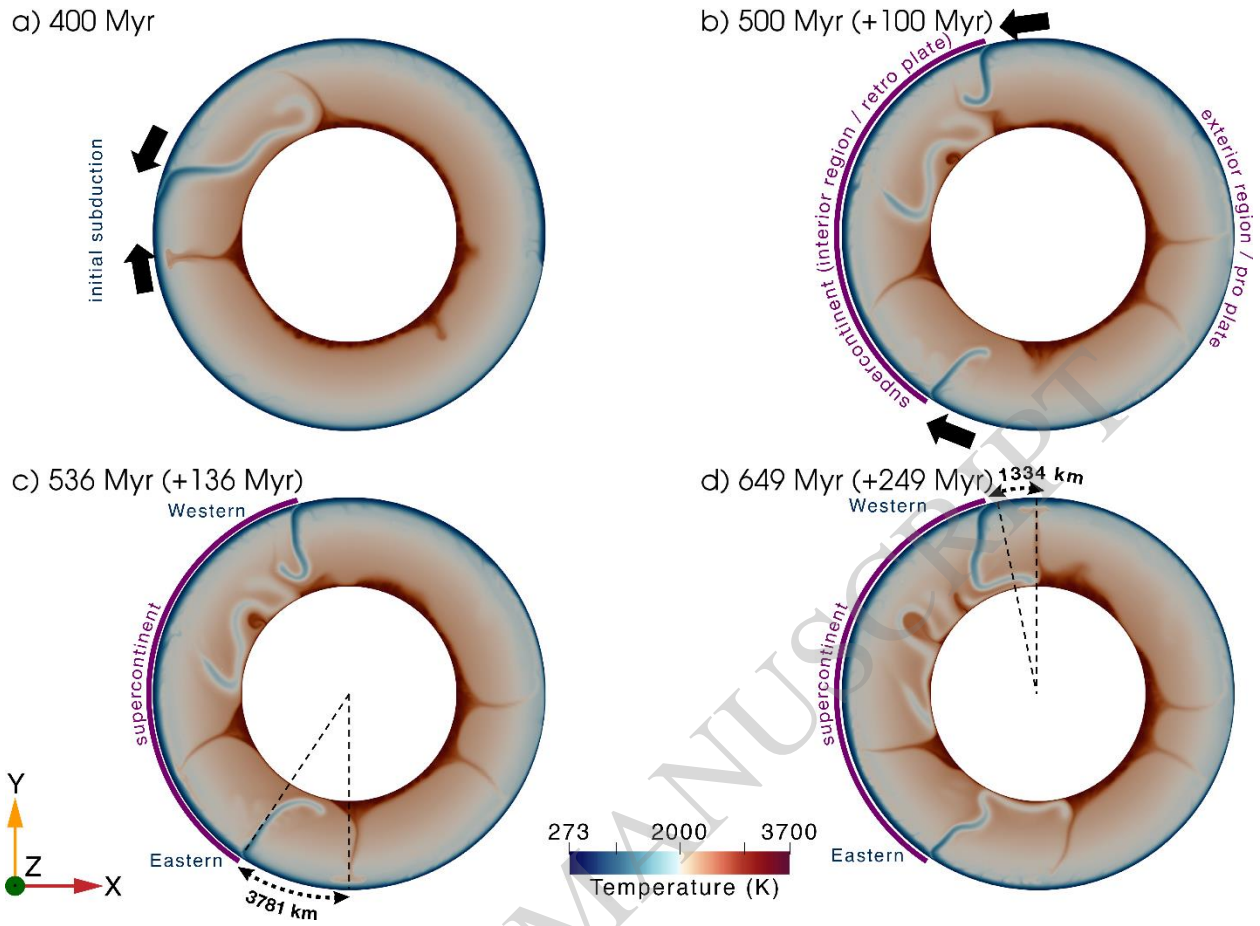

Figure 6

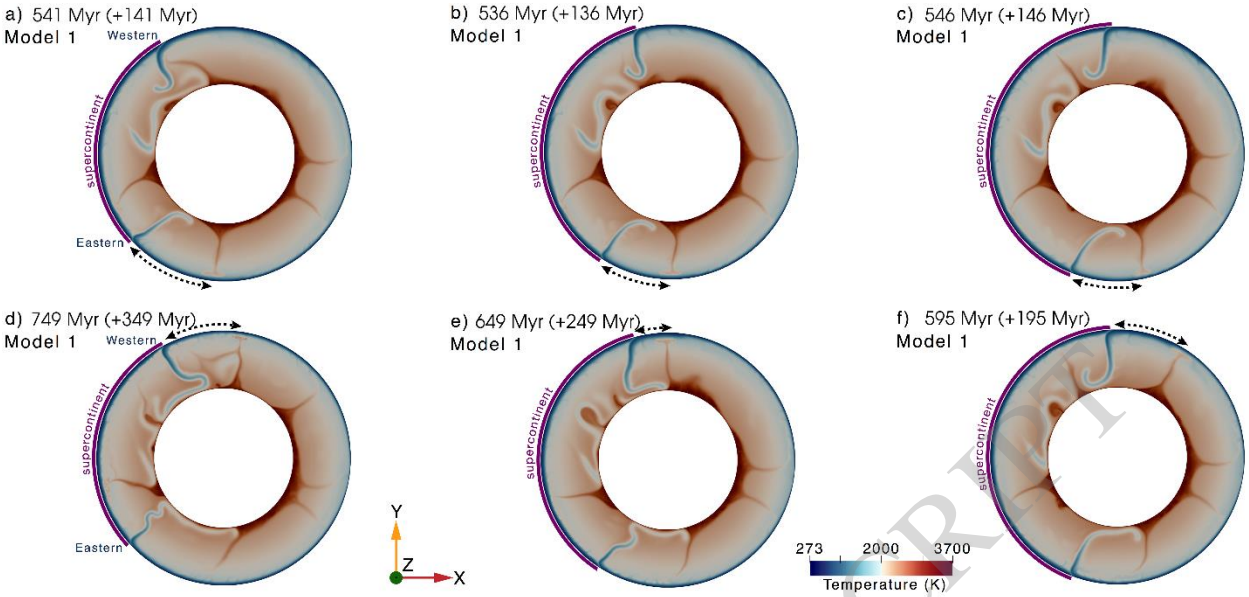

Figure 7

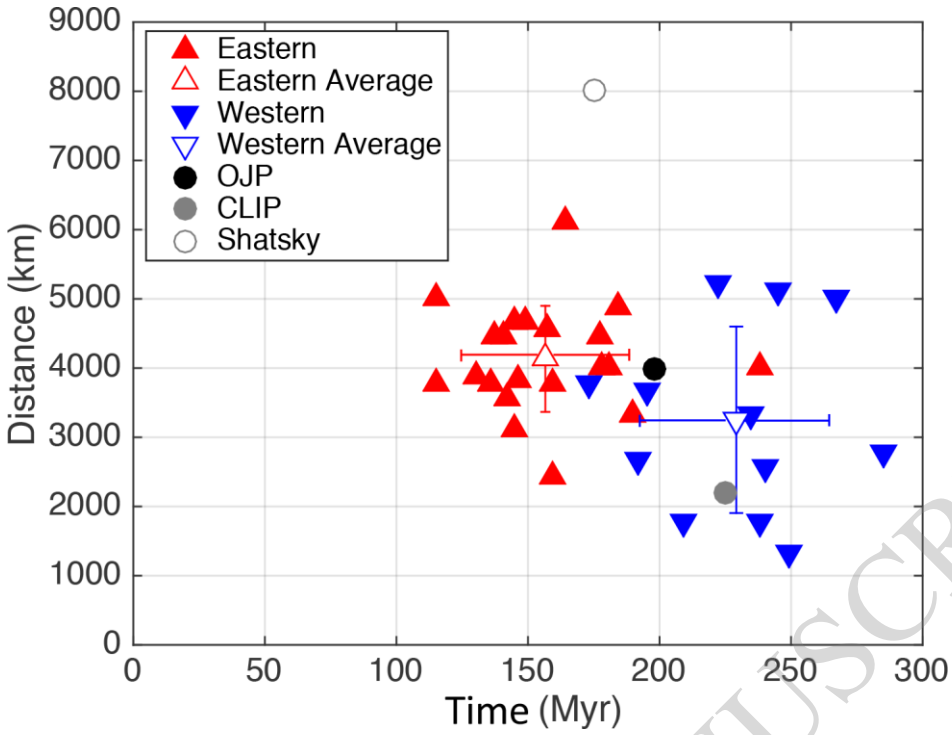

Figure 8

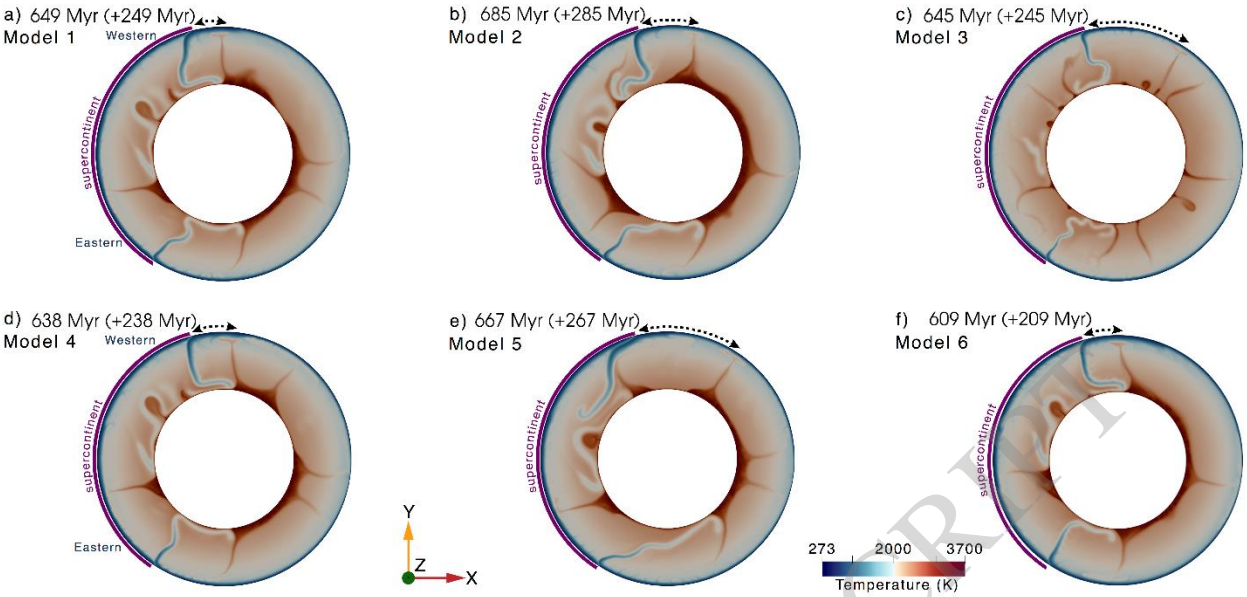

Figure 9

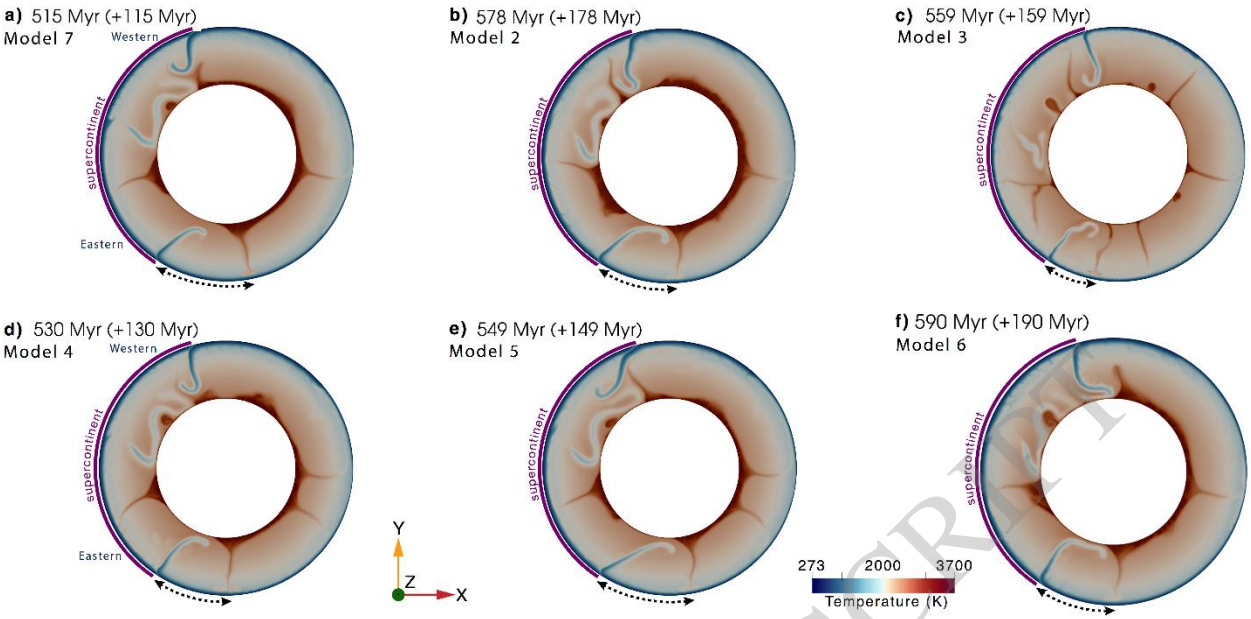

Figure 10

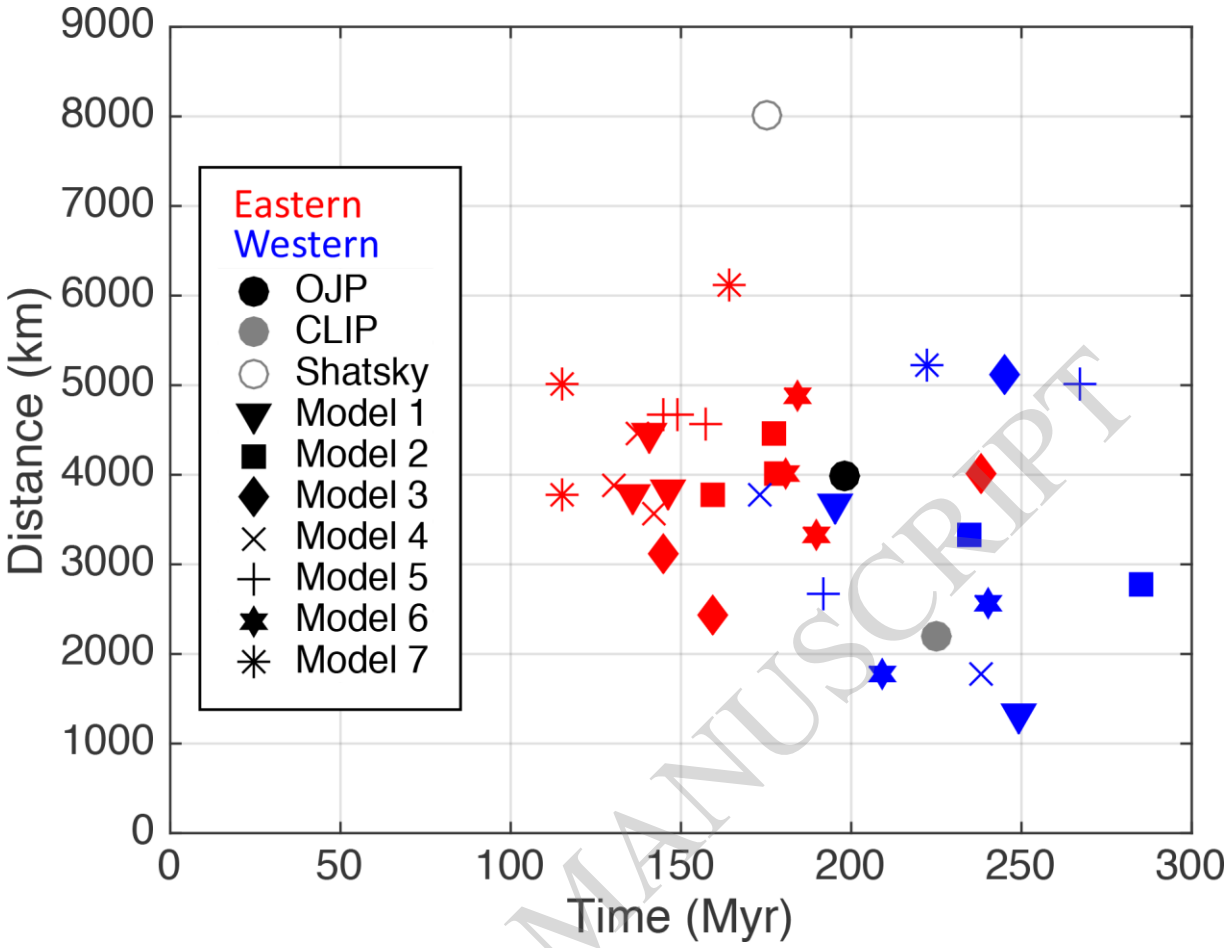

Figure 11

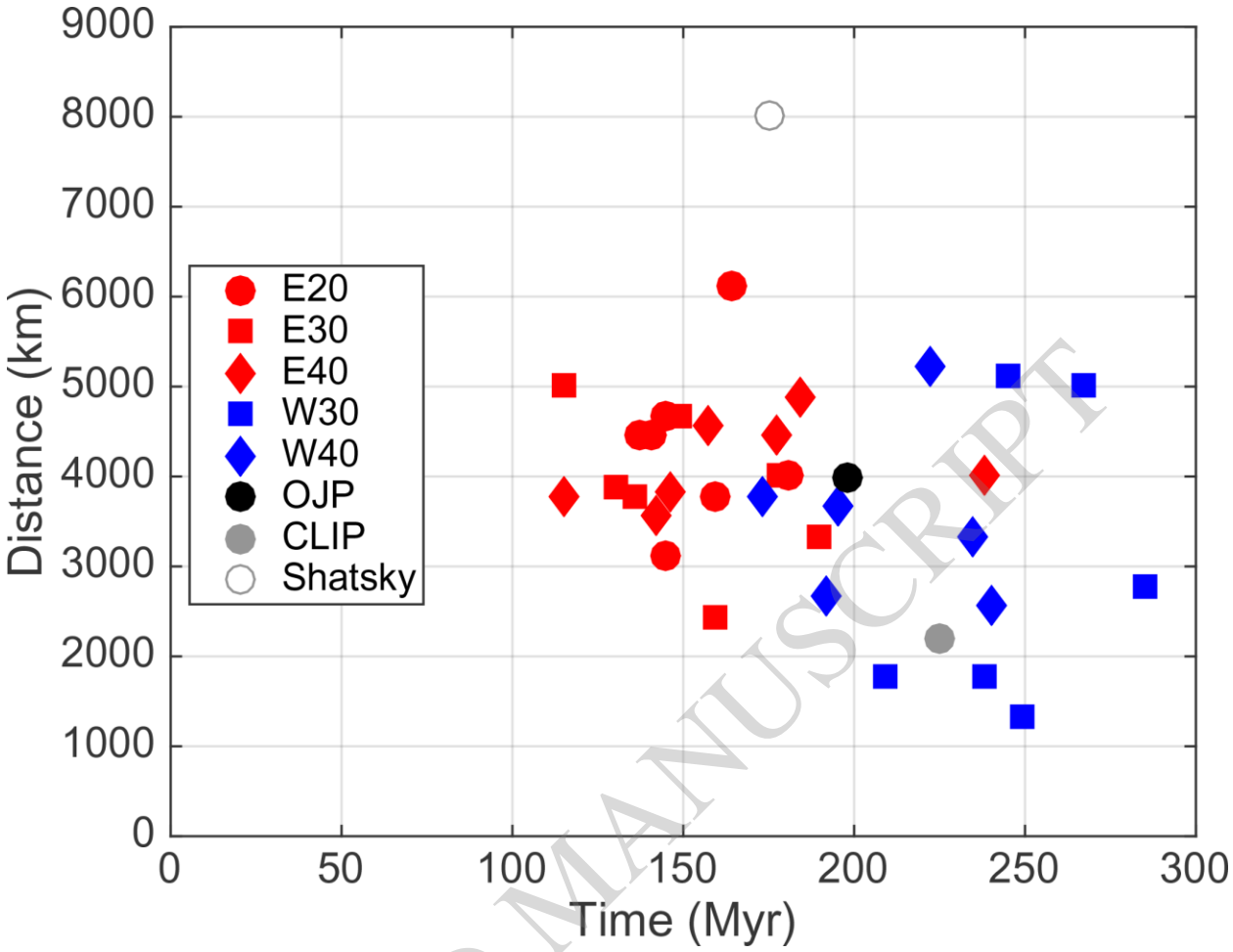

Figure 12

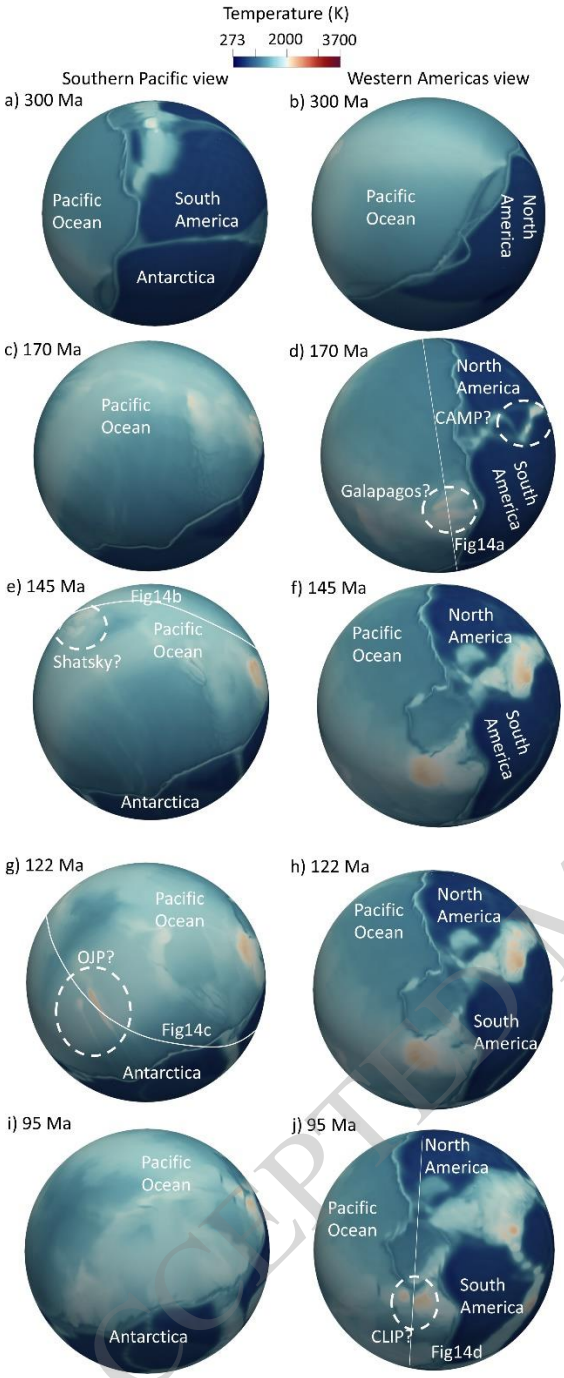

Figure 13

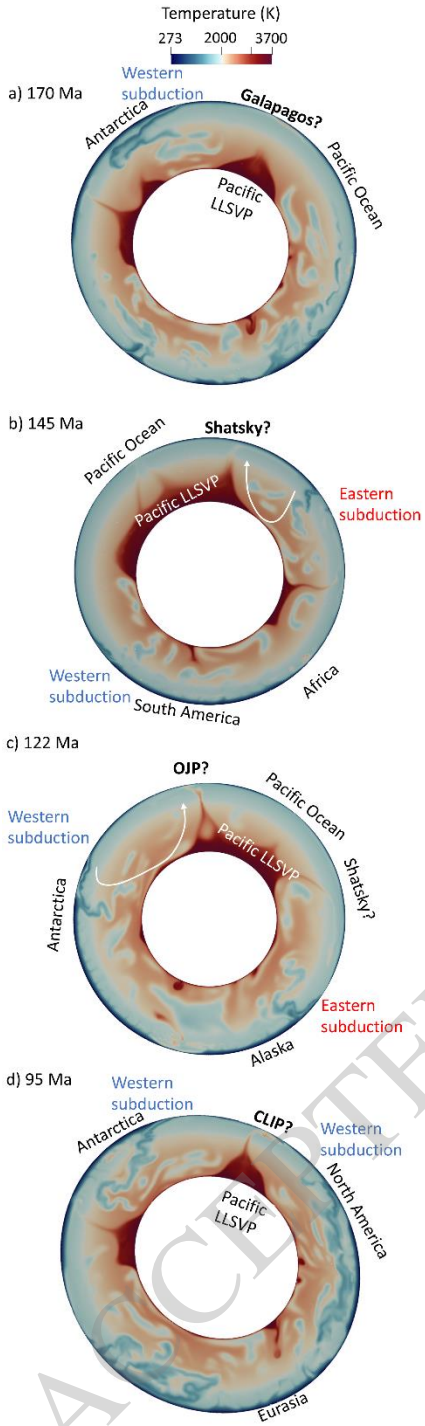

Figure 14